

1
2
3
4
5
6
7

Using SHAP to interpret XGBoost predictions of grassland degradation in Xilingol, China

Batunacun^{1,2*}, Ralf Wieland², Tobia Lakes^{1,3}, Claas Nendel^{2,3}

¹ Department of Geography, Humboldt-Universität zu Berlin, Unter den Linden 6, 10099 Berlin, Germany

² Leibniz Centre for Agricultural Landscape Research (ZALF), Eberswalder Straße 84, 15374, Müncheberg, Germany

³ Integrative Research Institute on Transformations of Human-Environment Systems, Humboldt-Universität zu Berlin, Friedrichstraße 191, 10099 Berlin, Germany

* Correspondence to: Institute of Landscape Systems Analysis, Leibniz Centre for Agricultural Landscape Research (ZALF), Eberswalder Straße 84, 15374, Müncheberg, Germany

E-mail: batunacun@zalf.de

8 Abstract

9 Machine learning (ML) and data-driven approaches are increasingly used in many research areas.
10 XGBoost is a tree boosting method that has evolved into a state-of-the-art approach for many ML
11 challenges. However, it has rarely been used in simulations of land use change so far. Xilingol, a
12 typical region for research on serious grassland degradation and its drivers, was selected as a case
13 study to test whether XGBoost can provide alternative insights that conventional land-use models
14 are unable to generate. A set of twenty drivers was analysed using XGBoost, involving four
15 alternative sampling strategies, and SHAP to interpret the results of the purely data-driven approach.
16 The results indicated that, with three of the sampling strategies (over-balanced, balanced and
17 imbalanced), XGBoost achieved similar and robust simulation results. SHAP values were useful for
18 analysing the complex relationship between the different drivers of grassland degradation. Four
19 drivers accounted for 99% of the grassland degradation dynamics in Xilingol. These four drivers
20 were spatially allocated, and a risk map of further degradation was produced. The limitations of
21 using XGBoost to predict future land-use change are discussed.

22 **Key words:** grassland degradation, machine learning, driver-driven method, XGBoost, SHAP
23 values

24 1. Introduction

25 Land-use and land-cover change (LUCC) has received increasing attention in recent years (Aburas
26 et al., 2019; Diouf & Lambin, 2001; Lambin et al., 2003; Verburg et al., 2002). Land-use change
27 includes various land-use processes, such as urbanisation, land degradation, water body shrinkage,
28 and surface mining, and has significant effects on ecosystem services and functions (Sohl &
29 Benjamin, 2012). Grassland is the major land-use type on the Mongolian Plateau; its degradation
30 was first witnessed in the 1960s. About 15% of the total grassland area was characterised as being
31 degraded in the 1970s, which rose to 50% in the mid-1980s (Kwon et al., 2016). In general,
32 grassland degradation (GD) refers to any biotic disturbance in which grass struggles to grow or can
33 no longer exist due to physical stress (e.g. overgrazing, trampling) or changes in growing conditions
34 (e.g. climate; Akiyama & Kawamura, 2007). In this study, grassland degradation is defined as
35 grassland that has been destroyed and subsequently classified as some other land use, or that has
36 significantly decreased in coverage.

37 Grassland is a land use that provides extensive ecosystem services (Bengtsson et al., 2019). When
38 degraded, the consequences are seen in an immediate decline in these services, such as a decrease
39 in carbon storage due to a reduction in vegetation productivity (Li et al., 2017). About 90% of carbon
40 in grassland ecosystems is stored in the soil (Nkonya et al., 2016). Furthermore, GD results in a
41 reduction in plant diversity and above-ground biomass available for grazing (Wang et al., 2014).
42 Likewise, GD leads to soil erosion and frequent dust storms in Inner Mongolia (Hoffmann et al.,
43 2008; Reiche, 2014). Drivers of GD are manifold, and have been analysed in a range of studies (Li
44 et al., 2012; Liu et al., 2019; Sun et al., 2017; Xie and Sha, 2012). However, few studies use
45 sophisticated driver analysis to predict spatial patterns of GD (Jacquin et al., 2016; Wang et al.,
46 2018). A number of studies have addressed the complex relationship between GD and its drivers
47 (Cao et al., 2013a; Feng et al., 2011; Fu et al., 2018; Tiscornia et al., 2019a). However, these studies
48 focus mainly on visualising or describing non-linear relationships between GD and its drivers.

49 The aim of developing various land-use models was to explore the causes and outcomes of land-use
50 dynamics; these models were implemented in combination with scenario analysis to support land
51 management and decision-making (National Research Council, 2014; Ren et al., 2019). Most such
52 models are statistical models, such as logistic regression models or models based on principle

53 component analysis (Li et al., 2013; Lin et al., 2014) or Bayesian belief networks (Krüger and Lakes,
54 2015). Some such models are spatially explicit (e.g. CLUE-S, GeoSOS-FLUS, LTM, Fu *et al.*, 2018;
55 Liang *et al.*, 2018; Pijanowski *et al.*, 2002, 2005; Verburg & Veldkamp, 2004; Zhang *et al.*, 2013);
56 others are not (e.g. Markov models; Iacono et al., 2015; Yuan et al., 2015). Hybrid models, which
57 combine different approaches to make the best use of the advantages of each model, are another
58 important variety. This type of model is used to characterise the multiple aspects of LUCC patterns
59 and processes (Li and Yeh, 2002; Sun and Müller, 2013). Agent-based models (ABM) simulate
60 land use change decisions based on the behaviour of individual decision-makers. They often
61 consider economic and political information to calculate land-use change. Cellular Automata (CA)
62 models are gridded models in which time, space, and state are all discrete. CA models are spatially
63 explicit and land use change decisions are made based on the state of the neighbouring cells (Yang
64 et al., 2014). CA models are often used for the spatial allocation of land use and land cover at a high
65 spatial resolution (Cao et al., 2019) and may be used in combination with other models, such as
66 ABM (e.g. Charif et al., 2017; Mustafa et al., 2017; Troost et al., 2015; Vermeiren et al., 2016).

67 In most cases of land-use change, it was either assumed that the relationship between the drivers
68 and the resulting land-use change is constant over time (Fu et al., 2018; Samie et al., 2017; Zhan J
69 Y et al., 2007), or the relationships were identified as being linear or non-linear, but were not
70 interpreted (Tayyebi and Pijanowski, 2014a). We hypothesise that the relationships between GD and
71 its drivers are mainly non-linear. We therefore see a need for methods that are capable of analysing
72 and interpreting non-linear relationships between GD and dynamic drivers.

73 With the development of computer science, machine learning (ML) models have been increasingly
74 used in land-use change modelling (Islam et al., 2018; Krüger and Lakes, 2015; Lakes et al., 2009;
75 Tayyebi and Pijanowski, 2014a). ML is superior to the human brain when it comes to pattern
76 recognition in large datasets, e.g. images and sensor fields. Once the task is defined and the data for
77 training is provided, ML operates without any further human assistance. Various ML approaches
78 have been used in the analysis of land-use change processes, the most prominent of which being
79 Support Vector Machines (SVM, Huang *et al.*, 2009, 2010), Artificial Neural Networks (ANN,
80 Ahmadlou *et al.*, 2016; Yang *et al.*, 2016), Classification And Regression Trees (Tayyebi and
81 Pijanowski, 2014b) and Random Forest (RF, Freeman *et al.*, 2016). While the different ML
82 approaches generally perform well in identifying patterns, they remain a black box and make no
83 contribution to our understanding of how the underlying drivers act on the LUCC process.
84 Compared to linear methods such as logistic regression, ML models often achieve higher accuracy
85 and capture non-linear land-use change processes. Likewise, ML models relax some of the rigorous
86 assumptions inherent in conventional models, but at the expense of an unknown contribution of
87 parameters to the outcomes (Lakes et al., 2009). However, the key challenge is to crack the black
88 box and reveal how each driver affects the land-use change pattern or processes in the ML models.

89 The eXtreme Gradient Boosting (XGBoost) method has recently been developed as a supervised
90 machine learning approach (Chen and Guestrin, 2016). XGBoost algorithms have achieved superior
91 results in many ML challenges; they are characterised by being ten times faster than popular existing
92 solutions, and the ability to handle sparse datasets and to process hundreds of millions of examples.
93 XGBoost has already been used in land-use change detection, combined with remote sensing data
94 (Georganos et al., 2018), but has not yet been used in the simulation and prediction of land-use
95 change. SHapley Additive exPlanations (SHAP; Lundberg & Lee, 2016) is a unified approach to
96 explain the output of any ML model and to visualise and describe the complex causal relationship
97 between driving forces and the prediction target. We propose using SHAP to analyse the driver
98 relationships hidden in the black box model of XGBoost when employed for land-use change
99 modelling.

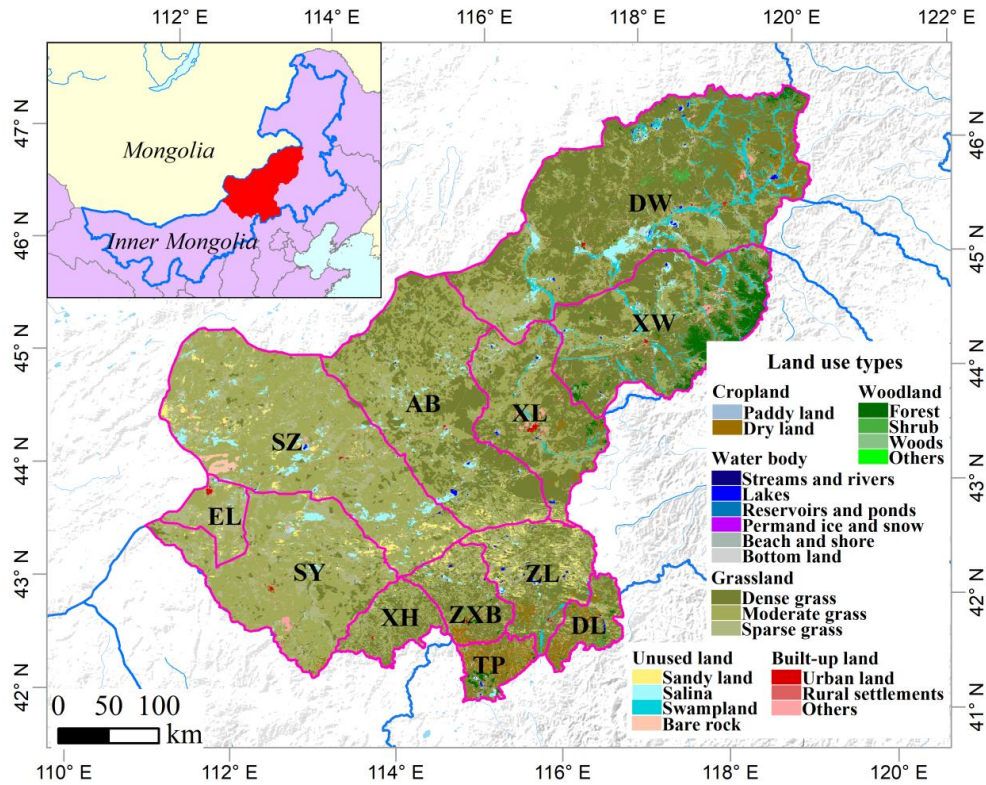
100 Having earlier used a clustering approach to identify drivers of GD in a case study in Inner Mongolia
101 (Xilingol League; Batunacun *et al.*, 2019), we now use XGBoost and SHAP to simulate GD
102 dynamics across the same area. We are primarily interested in learning whether ML models can

103 achieve a better predictive quality than linear methods, in addition to improving our understanding
104 of how grassland degrades in Xilingol. In the intention to identify areas with a high risk of further
105 degradation and to determine the drivers responsible for progressive degradation, we used XGBoost
106 to generate a data-driven model to explore the GD patterns. We then used SHAP to open the non-
107 linear relationships of the black box model stepwise, and transformed these relationships into
108 interpretable rules. The resulting model enabled us to map the primary GD drivers and GD hot spots
109 in Xilingol.

110 **2. Materials and Methods**

111 **2.1 Study area**

112 The Xilingol League is located about 600 km north of Beijing (He et al., 2004), in the centre of
113 Inner Mongolia. This administrative unit, covering an area of 206,000 km², spans from 41.4°N to
114 46.6°N and from 111.1°E to 119.7°E (Figure 1). The area is dominated by the continental temperate
115 semiarid climate. The frequent droughts (in summer) and “dzud” (an extremely harsh and snow-
116 rich winter) are the major natural disasters that occasionally lead to catastrophic livestock losses in
117 this region (Allington et al., 2018; Tong et al., 2017; Xu GC et al., 2014). Xilingol possessed about
118 18,104 km² available pasture resources and 1240.4·10⁴ sheep units at the end of 2015 (Xie and Sha,
119 2012). Around 1.044 million people lived in Xilingol in 2015, with ethnic Mongolian minorities
120 accounting for around 31% and the rural population for 37% (Batunacun et al., 2019; Shao et al.,
121 2017). Xilingol is a vast grassland, known for its high-quality meat products, nomadic culture, rich
122 mineral resources and ethnic minorities. The ongoing degradation of grassland is receiving
123 increasing attention. A set of economic stimuli and ecological protection policies launched in
124 Xilingol were viewed as the root cause of GD over the past four decades. Although large-scale
125 ecological restoration policies were implemented after 2000 in a bid to reduce GD, the problem still
126 persists.



127

128 Figure 1: The location of the Xilingol League in Inner Mongolia and its land uses.

129 **2.2 Grassland degradation**

130 This study defines grassland degradation (GD) based on land-use conversion, involving two kinds
 131 of land-use change processes: (i) the complete destruction of grassland by transformation to another
 132 type of land use (built-up land, cropland, woodland, water bodies and unused land), and (ii) a decline
 133 in grassland coverage, which includes dense grass deteriorating into moderately dense grass and
 134 sparse grass, and moderately dense grass deteriorating into sparse grass (see Fig. S 1a). Given that
 135 GD is a dynamic process, we intended in this study to find the major drivers of newly added
 136 grassland degradation (NGD). NGD refers to the difference in spatial GD extent between two
 137 periods. About 13.0% of the total grassland area (176,410 km² in 2015) was degraded between 1975
 138 and 2000 (Fig. S 1b); a further 10.6% was degraded in 2000-2015 (Fig. S 1c). Comparing the two
 139 periods, approximately 10.2% of the grassland corresponded to the NGD area across the whole
 140 region (Fig. S 1d). 18,093 pixels were extracted from the total NGD area, while the pixel number
 141 of conversion for other land uses is 178,990 in this study (hereafter: non-NGD).

142 **2.3 Data collection**

143 In line with previous studies, a checklist of possible drivers (D) of GD was developed from the literature
 144 (Cao et al., 2013b; Sun et al., 2017). A total of 19 drivers were grouped into four categories (see Table
 145 1). All categories were described as follows: (1) Climate factors, including the annual mean temperature
 146 (T) and annual sum of precipitation (P) in the growing season (April to Sep), were extracted from the
 147 longest available weather dataset (from 1958-2015), in combination with evaluation data and the kriging
 148 algorithm, to produce 1×1 km² raster files. (2) Geographic factors include elevation (DEM), and slope
 149 and aspect (extracted from DEM data), which can be treated as the characteristic of each grid cell. The
 150 DEM data were extracted from the SRTM 90m resolution and, after resampling using the NEAREST

151 method in ArcGIS, all data were processed into 1×1 km² raster files. (3) Distance measures (the distance
152 of each pixel centre to urban, rural, road and mining, forest, cropland, dense grass, moderately dense
153 grass, sparse grass and unused land pixels) are widely used factors for different land-use models (Khoury,
154 2012; Samardžić-Petrović et al., 2016, 2017; Zhang et al., 2013). All distance measures were extracted
155 from LUCC datasets from the years 2000 and 2015 using ArcGIS Euclidean distance, and processed into
156 1×1 km² grids. (4) Socio-economic factors include the gross domestic product (GDP) and population
157 density from 2000 and 2010, and sheep density from 2000 and 2015. GDP and population density were
158 obtained from a resources and environment data cloud platform, CAS (<http://www.resdc.cn/>); sheep
159 density data were accessed from statistical data; and we converted all livestock data into grassland pixels.
160 Unfortunately, high-resolution GDP and population density data was not available for 2015 to match the
161 other data that was recorded for that year, so we may assume that GDP and population density introduce
162 a bias to the result. While population density did not change much between 2010 and 2015, GDP changed
163 from 61.4 billion Yuan in 2010 to 100.2 billion Yuan in 2015 in total over the Xilingol region (GDP data
164 source: <http://tjj.xlgl.gov.cn/ywlm/tjsj/jdsj/>). (5) Finally, we identified an area in which we assumed
165 a strong policy impact in the past, and developed a proxy for the policy effect on grassland degradation.
166 Here, a range of ecological protection measures were implemented inside and outside the Hunshandake
167 and Wuzhumuqin sand lands (see Fig. S 2), e.g. a livestock ban and the promotion of chicken farming
168 (Su et al., 2015). In a bid to explore policy effects, we assumed that GD is effectively slowed down by
169 various policies inside the sandy area (proxy set as 0), while outside the sandy area, land degradation is
170 more likely to happen in the absence of any policy effect (proxy set as 1, see Fig. S 2).

171 Table 1: Definition and derivation of drivers

Code	Name of driver	Definition of driver	Unit	Measures	Time series	Original format	Process approach	Data sources
Climate factors								
F1	temperature	Difference between average temperature / total precipitation in growth season (April-September) in Phase 1* and Phase 2*	°C	Mean temperature	2000, 2015	Grid	Kriging via ArcGIS and Python language	National Meteorological Information Center (https://data.cma.cn/)
F2	precipitation		mm	cumulative rainfall	2000, 2015			
Geographic factors								
F3	DEM	DEM	m	--		Grid	--	STRM
F4	slope	slope	degree	--		Grid	Reclassification	http://srtm.csi.cgiar.org/SELECTION/inputCoord.asp
F5	aspect	aspect	degree	--		Grid	Reclassification	
Distance measures								
F6	discrop	Change of distance to cropland in 2000 and 2015	m	Distance	2000, 2015	SHP	Euclidean	Extraction from land-use data
F7	disforest	Change of distance to forest in 2000 and 2015	m	Distance	2000, 2015			
F8	disunused	Change of distance to unused land 2000 and 2015	m	Distance	2000, 2015			
F9	disdense	Change of distance to dense grass 2000 and 2015	m	Distance	2000, 2015			
F10	dismode	Change of distance to moderate grass in 2000 and 2015	m	Distance	2000, 2015			
F11	dis sparse	Change of distance to sparse grass 2000 and 2015	m	Distance				
F12	disurban	Change of distance to urban in 2000 and 2015	m	Distance	2000, 2015			
F13	disrural	Change of distance to rural in 2000 and 2015	m	Distance	2000, 2015			

F1 4	disroad	Change of distance to road in 2000 and 2015	m	Distance	2000, 2015			
F1 5	dismine	Change of distance to mining in 2000 and 2015	m	Distance	2000, 2015			
F1 6	diswater	Change of distance to water in 2000 and 2015	m	Distance	2000, 2015			
Social-economic factors								
F1 7	population density	Change of population density in 2000 and 2010	Person	Person/ km2	2000, 2010	Grid	Density	Resource and Environment data cloud platform, CAS. (http://www.resdc.cn/)
F1 8	GDP*	Change of GDP in 2000 and 2010	Yuan	Yuan/km2	2000, 2010	Grid	Density	
F1 9	sheep density	Change of sheep density in 2000 and 2015	Sheep Unit	Sheep unit/km2	2000, 2015	Grid	Density	
Scenario setting								
F2 0	policy	--	--	(0,1)	--	Grid	--	Assumption

172 *Note: Phase 1 refers to 1975-2000; Phase 2 refers to 2000-2015. GDP: gross
173 domestic product.

174 2.3.1 XGBoost and logistic regression

175 Two algorithms were selected in this study: logistic regression (LR) and XGBoost. LR is a linear
176 method involving two parts: the statistic LR and the classification LR. Both methods have already
177 been used to simulate land use (Lin et al., 2011; Mustafa et al., 2018) and to define the relationship
178 between land-use change and its drivers (Gollnow and Lakes, 2014; Mondal et al., 2014; Verburg et
179 al., 2002; Verburg and Chen, 2000). Here, we use LR as a benchmark model to compare linear and
180 non-linear methods in the simulation of land-use change. The optimised parameters of LG are $C =$
181 0.1 , $\text{penalty} = l2$, $\text{solver} = \text{'lbfgs'}$, $\text{multi_class} = \text{'multinomial'}$.

182 Boosting algorithms have been implemented in many past studies, where they often outperformed
183 other ML algorithms (Ahmadlou et al., 2016; Filippi et al., 2014; Freeman et al., 2016; Keshtkar et
184 al., 2017; Tayyebi and Pijanowski, 2014a). However, traditional boosting algorithms are often
185 subject to overfitting (Georganos et al., 2018). To overcome this problem, Chen and Guestrin (2016)
186 presented a new, regularised implementation of gradient boosting algorithms, which they called
187 XGBoost (eXtreme Gradient Boosting). XGBoost was built as an enhanced version of the gradient
188 boosting decision tree algorithm (GBDT), a regression and classification technique developed to
189 predict results based on many weak prediction models – the decision tree (DT) (Abdullah et al.,
190 2019; Freeman et al., 2016). XGBoost provides strong regularisation by adopting a stepwise
191 shrinkage process instead of the traditional weighting process provided by GBDT. This process
192 limits overfitting, minimises training losses and reduces classification errors while developing the
193 final model (Abdullah et al., 2019; Hao Dong et al., 2018).

194 The XGBClassifier uses the following parameters: learning_rate (controls learning itself);
195 max_depth (control depth of the RF); the n_estimators (controls the number of estimators used for
196 the model); the min_child_weight (controls the complexity of a model, defines the minimum sum
197 of weights of all observations required in a child); and lambda (L2 regularisation term on weights).
198 The parameters were optimised using a simple grid search algorithm provided by scikit (Pedregosa
199 et al., 2011) to estimate the optimal parameters ($\text{learning_rate} = 0.1$, $\text{max_depth} = 9$, $\text{n_estimator} =$
200 500 , $\text{min_child_weight} = 3$, $\text{lambda} = 10$).

201 2.3.2 Sampling methods

202 Data are often distributed unevenly among different classes (Vluymans, 2019). Such imbalanced
203 class distribution generally induces a bias. Canonical ML algorithms assume that data is roughly
204 balanced in different classes. In real situations, however, the data is usually skewed, and smaller
205 classes often carry more important information and knowledge than larger ones (Krawczyk, 2016).
206 It is therefore important to develop learning from imbalanced data to build real-world models
207 (Krawczyk, 2016; Vluymans, 2019). To ensure a highly accurate GD model, we introduced four
208 different sampling methods in this study (Fig. S 3).

209 **Balanced sampling:** Random data sampling, resulting in equal sized samples.

210 **Imbalanced sampling:** Random data sampling, but with the same share of the sampled class,
211 resulting in unequal sized samples.

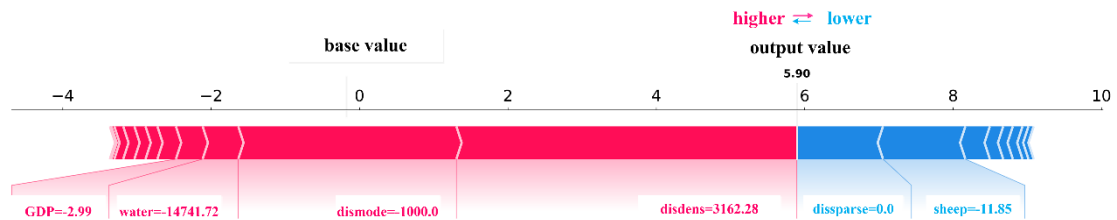
212 **Over-sampling:** Artificial points are added to the minority class of an imbalanced sampling set,
213 making it equal to the majority class and resulting in equal sized samples.

214 **Under-sampling:** Points are removed from a majority class of an imbalanced sampling set,
215 making it equal to the minority class and resulting in equal sized samples (He and Garcia, 2009).

216 In the present study, we used these four sampling methods to evaluate the model in the context of
 217 the sampling method and its performance in the training process and the simulation process (see Fig.
 218 S 3). In our case study, 20,000 pixels (about 10% of the total; including 18,190 pixels with value 0
 219 indicating no-change areas and restored grassland and 1,810 pixels with value 1 indicating newly
 220 added grassland degradation) were selected by different sampling methods (Fig. S 3) to train (66%
 221 of the sample size) and test (34% of the sample size) the model.

222 2.3.3 SHAP values

223 SHAP (SHapley Additive exPlanations) is a novel approach to improve our understanding of the
 224 complexity of predictive model results and to explore relationships between individual variables for
 225 the predicted case (Lundberg and Lee, 2017). SHAP is a useful method to sort the driver's effects,
 226 and break down the prediction into individual feature impacts. Feature selection is of primary
 227 concern when using ML methods to process land-use change (Samardžić-Petrović et al., 2015, 2016,
 228 2017). SHAP values show the extent to which a given feature has changed the prediction, and allows
 229 the model builder to decompose any prediction into the sum of the effects of each feature value and
 230 explain – in our case – the predicted NGD probability for each pixel (see Figure 3). In this study,
 231 we used SHAP values to sort the driver's attributions; capture the relationship between drivers and
 232 NGD; and map the primary driver for NGD at the pixel level.



233

234 Figure 2: Decomposed SHAP values for the individual prediction of an example pixel.

235 In our study, we define the *base value* as the value that would be predicted by the model if no feature
 236 knowledge were provided for the current output (mean prediction); we define the output value as
 237 the prediction for this particular observation. SHAP values are calculated in log odds. Features that
 238 increase the value of the prediction (to the left in Fig. 2) are always shown in red; those that lower
 239 the prediction value are shown in blue (to the right in Fig. 2, Dataman, 2019). In this instance (Figure
 240 2), *disdense* (change of distance to dense grass) is the primary driver of NGD at this pixel level
 241 (largest value). The fact that the value is positive means that the risk of NDG increases in line with
 242 an increase in distance to dense grass areas.

243 2.3.4 Validation of the model

244 Two validation steps are required for ML models: validation of the training process, and validation
 245 of the simulation process. For the training process, a robust model was selected using overall
 246 classification accuracy, precision, recall and the kappa index. Accuracy, precision and recall were
 247 calculated based on a confusion matrix (CM) (He and Garcia, 2009). For the simulation process, the
 248 final model was validated using the kappa index, the area under the precision-recall curve, and recall.
 249 The validation indicators are defined as follows.

250 Overall classification accuracy (ACC) is the correct prediction of NGD and other pixels in the whole
 251 region. This indicator was used to evaluate the accuracy of the model. Precision is the proportion of
 252 correctly predicted positive examples (refers to NGD in this study) in all predicted positive examples.
 253 Recall is the proportion of correctly predicted positive examples in all observed positive examples
 254 (the observed NGD) (Sokolova and Lapalme, 2009). In general, high precision predictions have a

255 low recall, and vice versa, depending on the predicted goals. Here, since we focus on NGD and
 256 other land-use changes, we use both indicators to evaluate our models.

257 Table 2: Confusion matrix for binary classification of newly added grassland degradation (NGD) and
 258 other changes, including four indicators: false positives (FP), cells that were predicted as non-change but
 259 changed in the observed map; false negatives (FN), cells that were predicted as change, but did not
 260 change in the observed map for disagreement; true positives (TP), cells that were predicted as change
 261 and changed in the observed map; and true negatives (TN), cells that were predicted as non-change and
 262 did not change in the observed map for agreement.

Simulated values	Observed values			Recall=TP/ (TP+FN)
	Others	NGD	Others	
Others	NGD	True negatives (TN)	False positives (FP)	Precision =TP/(TP+FP)
		False negatives (FN)	True positives (TP)	
ACC=(TP+TN)/(TP+FN+FP+TN)				

263 The precision-recall curve (PR curve) provides more information about the model’s performance
 264 than, for instance, the Receiver Operator Characteristic curve (ROC curve), when applied to skewed
 265 data (Davis and Goadrich, 2006). The PR curve shows the trade-off of precision and recall, and
 266 provides a model-wide evaluation. The area under the PR curve (AUC-PR) is likewise effective in
 267 the classification of model comparisons. The baseline for the PR curve (y) is determined by positives
 268 (P) and negatives (N). In our study, $y = 0.09$ ($y = 18374/200652$), which means when AUC-PR =
 269 0.09, the model is a random model (Brownlee, 2018; Davis and Goadrich, 2006).

270 The kappa index (κ) is a popular indicator used to measure the proportion of agreement between
 271 observed and simulated data, especially to measure the degree of spatial matching. When $\kappa > 0.8$,
 272 strong agreement is yielded between the simulation and the observed map; $0.6 < \kappa < 0.8$ describes
 273 high agreement; $0.4 < \kappa < 0.6$ describes moderate agreement; and $\kappa < 0.4$ represents poor agreement
 274 (Landis and Koch, 1977).

275 In this study, κ was used to evaluate the agreement and disagreement between observed NGD and
 276 simulated NGD. Kappa should be the primary validation measure, followed by AUC-PR (used to
 277 evaluate model performance) and recall (used to evaluate model sensitivity). Features and
 278 definitions of these indicators are given below.

279 2.3.5 The structure of the ML model

280 The ML methodology of simulating GD involves six steps (Fig. S 4): (1) Target definition and data
 281 collection and processing; the targets of this study are to build a robust ML model for simulating
 282 NGD, as well as visualising these complex relationships between various variables and the dynamics
 283 of GD. A total of 20 drivers (D) of GD were collected. All dynamic drivers were processed by GIS
 284 into raster files and exported into ASCII files as final inputs for the ML model. (2) Data organisation:
 285 the ML model simulates land-use change as a classification task (Samardžić-Petrović et al., 2015,
 286 2017). In the present study, we organise this task as a binary classification Y (value 1 and 0, stand
 287 for NGD and Non-NGD); related drivers are x ($x_1, x_2, x_3, \dots, x_n$), n is the driver identifier, and x
 288 denotes the change in value of each driver. The process of data standardisation is usually necessary
 289 for most ML models, but since XGBoost is a tree-based method, it does not require standardisation
 290 or normalisation. In this case, we performed standardisation only for the logistic regression model.
 291 (3) Data sampling: this is a necessary step to avoid overfitting or the loss of important information.
 292 The sampling method generally includes balanced and imbalanced sample strategies. In this study,
 293 we tested various balanced sampling strategies to identify the most suitable one. (4) Model building
 294 and selection: a ranking was used to find the best model in each specific case. In our study, we

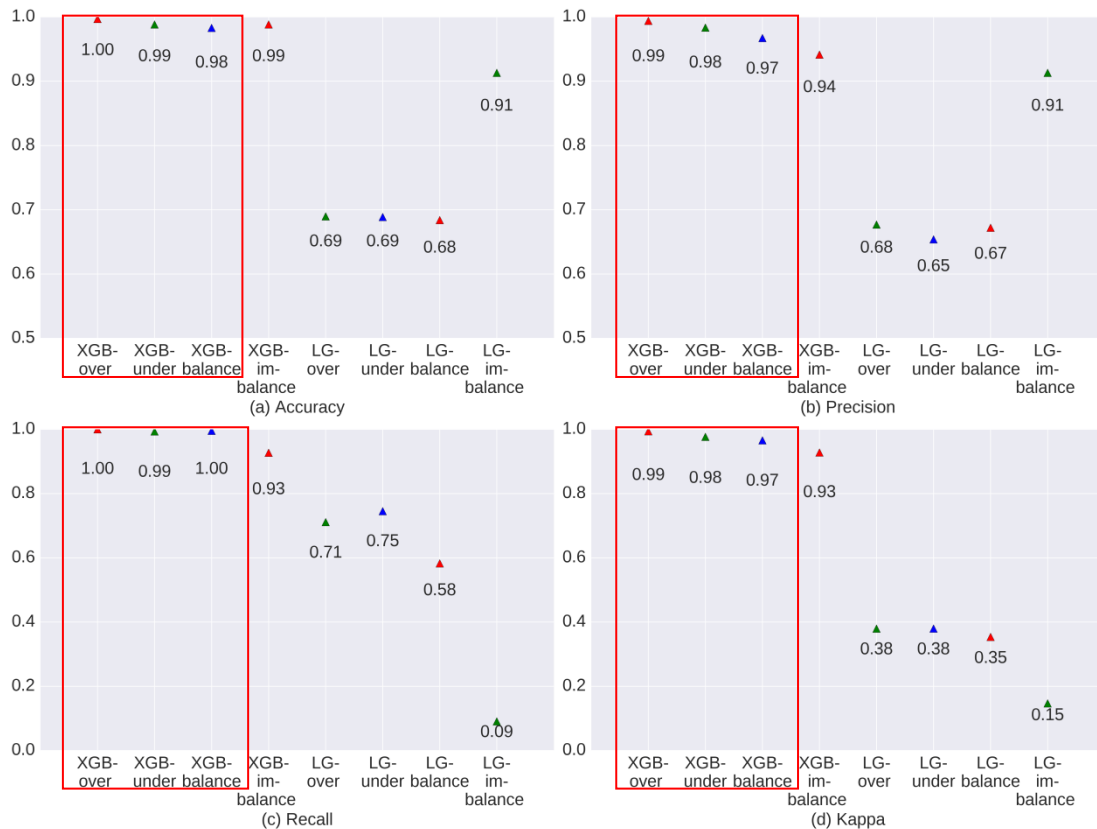
295 defined a model with $\kappa > 0.8$ and $AUC-PR > 0.09$ as robust, while $0.6 < \kappa < 0.8$ and $AUC-PR > 0.09$
 296 represents an acceptable model. (5) Model validation and feature ranking: after tuning the model,
 297 the most robust model and the driver with most useful information are selected. (6). The last step is
 298 explaining the model and the simulation. The model used in training process was published in
 299 ZENODO (Batunacun and Ralf Wieland, 2020)

300 3. Results

301 3.1 Model validation

302 The XGBoost model outperformed the LG model in both training and simulation (Figure 3 and 4).
 303 The LG model seems to be an inappropriate model for understanding NGD in this case. XGBoost
 304 yielded robust results in both training and simulation, with indicator values almost entirely above
 305 90%.

306 Figure 3 indicates that XGBoost performed very well across all balanced sampling methods (over-
 307 sampling, under-sampling and balanced sampling, red rectangle in Figure 3) in the training process.
 308 Only the imbalanced sampling exhibited a slightly weaker performance in the training process. This
 309 is mainly due to the balanced sampling datasets, which provided more information for the model.
 310 In addition, the model was affected less than the imbalanced sampling method by the majority class
 311 or unchanged cells (Mileva Samardzic-Petrovic et al., 2018).

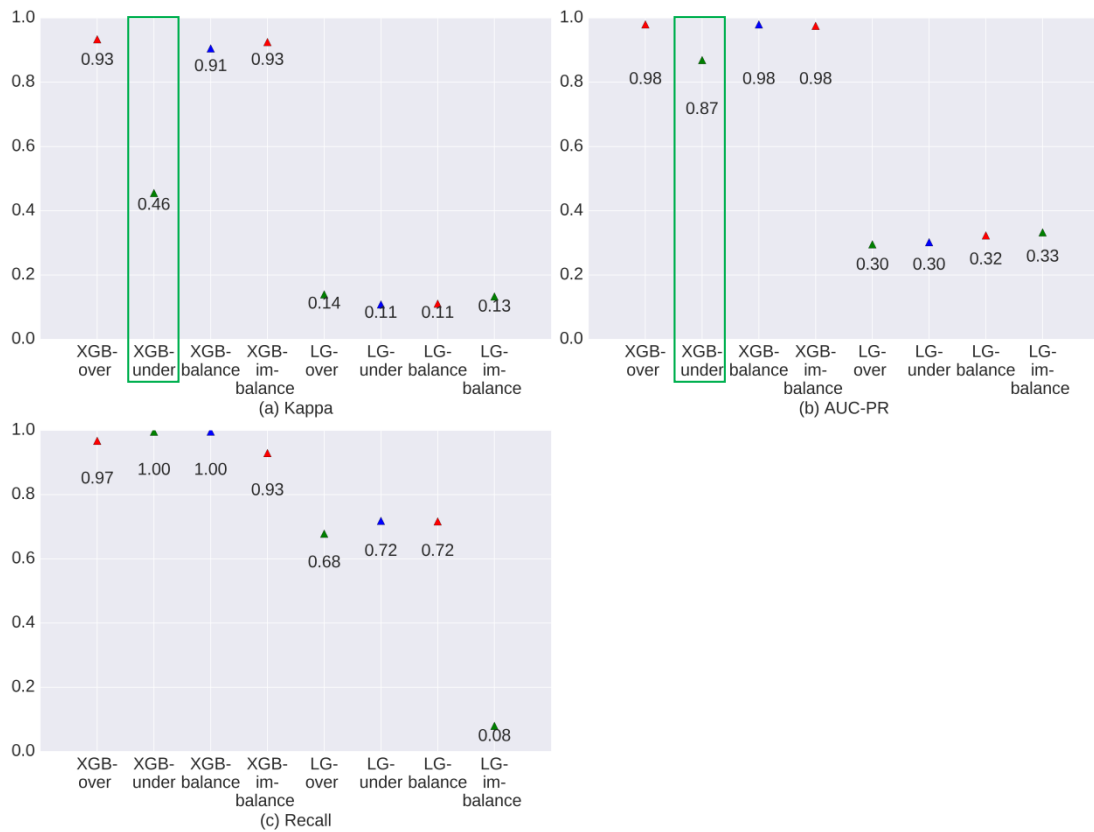


312

313 Figure 3: Evaluation of model performance during the training process for newly added grassland
 314 between 1975–2015.

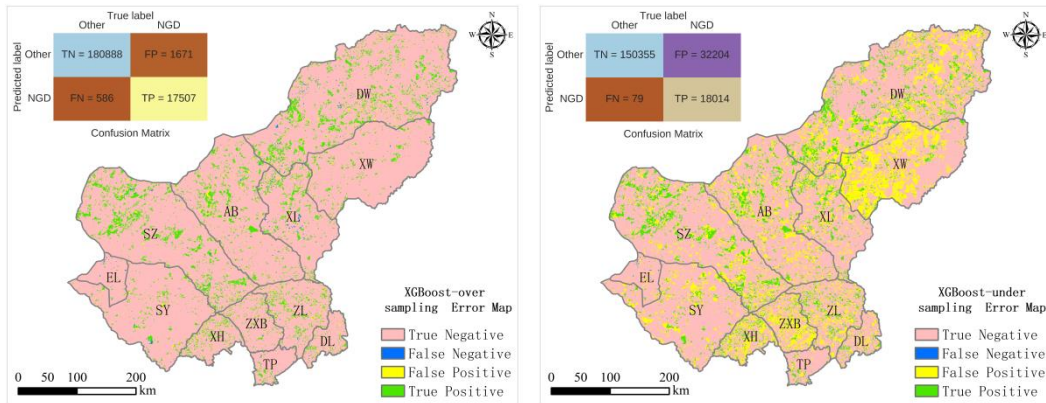
315 Figure 4 and Figure 5 show the model evaluation results in the simulation process and the spatial
 316 prediction maps. XGBoost with under-sampling (green rectangle in Figure 4) yielded the weakest
 317 performance compared to the other three sampling methods. This is mainly due to the smaller
 318 sample size, which prevents the model from extracting sufficient experience. As can be seen in
 319 Figure 5b, XGBoost used with the under-sampling method produced the error map with the highest
 320 FP values, where the model predicted non-change points as change points. The under-sampling
 321 method is unable to identify NGD points sufficiently well. XGBoost used with the over-sampling
 322 method caused balanced and imbalanced sampling to have similar and strong prediction abilities
 323 (see Figure 4), differing only slightly in their CM indicators (see Figure 5). We finally selected
 324 XGBoost combined with the over-sampling strategy for our study, mainly because of its relatively
 325 higher values in κ , AUC-PR and recall (see Figure 4).

326



327

328 Figure 4: Evaluation of model performance during the prediction process for newly added grassland
 329 between 1975–2015.

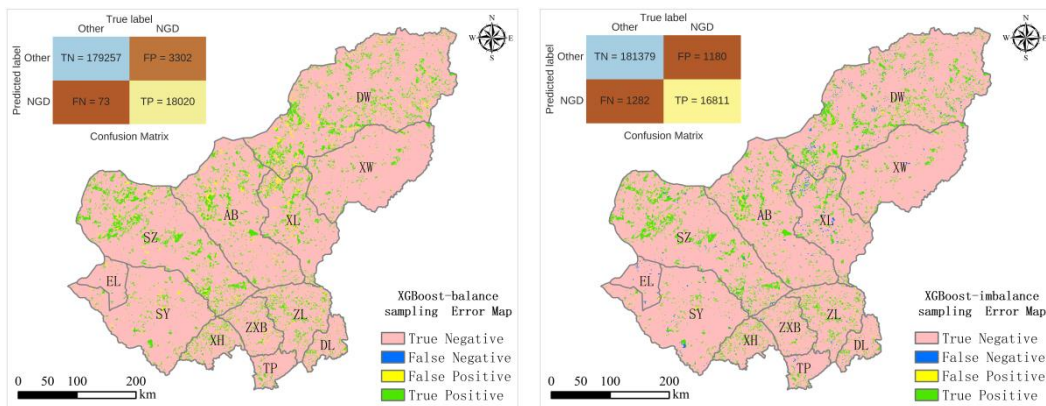


330

331

(a) Over-sampling

(b) Under-sampling



332

333

(c) Balanced sampling

(d) Imbalanced sampling

334

Figure 5: Error map of different sampling methods using the XGBoost model.

335

3.2 Driver selection

336

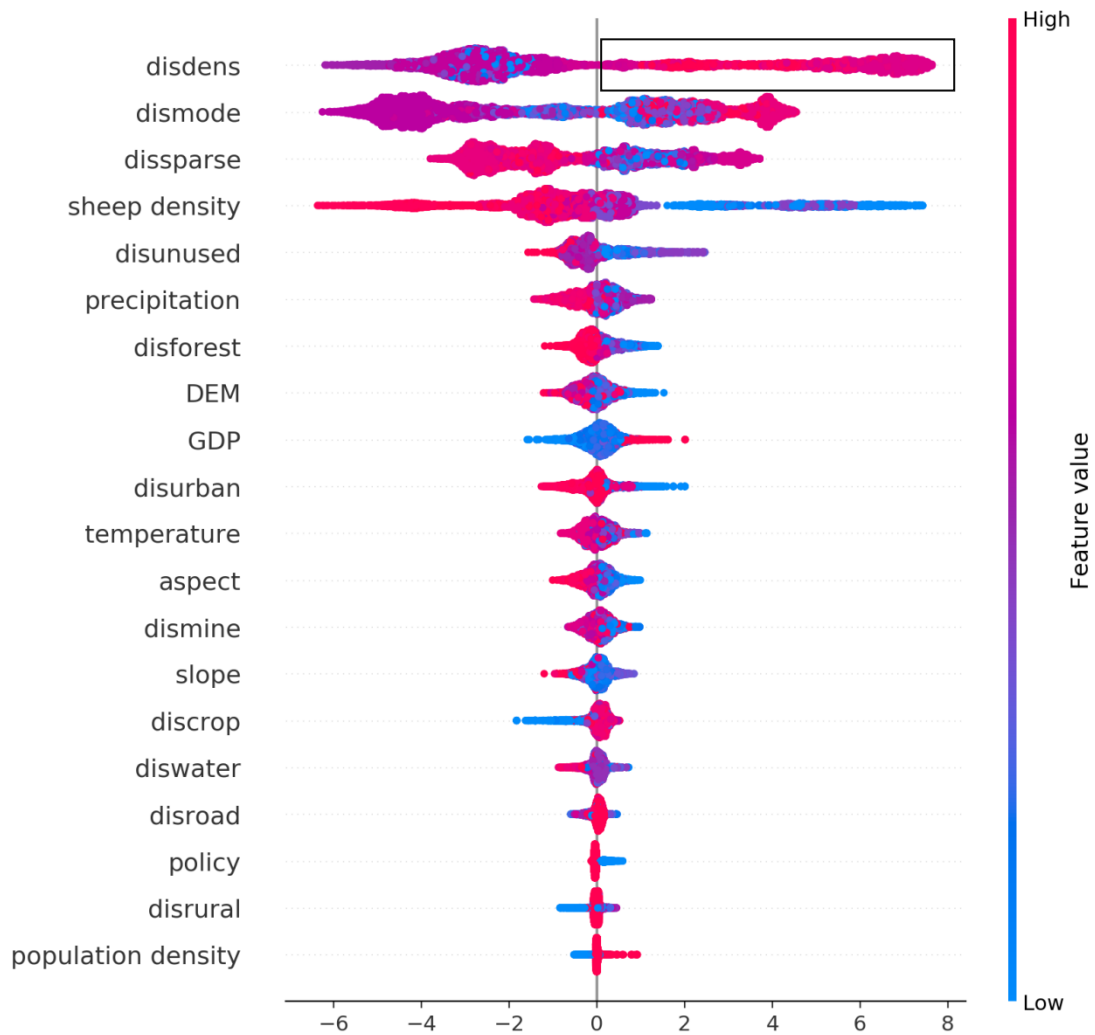
Figure 6 is a summary plot produced from the training dataset; it includes approximately 13,200 points (66% of the sample size). This plot combines feature importance (drivers are ordered along the y-axis) and driver effects (SHAP values on the x-axis), which describe the probability of NGD having occurred. Positive SHAP values refer to a higher probability of NGD. The gradient colour represents the feature value from high (red) to low (blue), as previously introduced in Figure 2. As Figure 6 shows, *disdense* was the primary driver for NGD in the study region. The relationship between *disdense* and NGD is non-linear, which can be seen from the SHAP values being both positive and negative (black rectangle in Figure 6). The interpretation of the effects of *disdense* can be summarised as a higher probability of NGD with increasing distance from dense grassland (see black rectangle in Figure 6 with pink colour on the right).

346

Figure 6 shows that driver effects include both linear-dominated relationships, such as *sheep*, *GDP* and others, and non-linear-dominated relations, such as *disdense*, *dismode* and others. In addition, the figure shows that the most important drivers for NGD are the changes of distance to dense, moderately dense and sparse grassland, then followed by sheep density and the distance to unused land. The effect of policies comes almost at the bottom, indicating that policies implemented outside sandy areas seem to have little effect on GD. The geographical factors DEM and slope are also positioned mid-field. The effect of geographical drivers does not appear to be as strong as the effect

352

353 of other drivers. The change of distance to mining, located at the bottom for all drivers, does not
 354 have a strong effect on NGD compared to other drivers.



355
 356 Figure 6: Driver ranking by SHAP values based on the training dataset (66% of sample size) using the
 357 over-sampling method.

358 Note: The top rank indicates the most significant effects across all predictions. Each point in the cloud to
 359 the left represents a row from the original dataset. The colour code denotes high (red) to low (blue) feature
 360 values. Positive SHAP values represent a higher likelihood of NGD, while negative values indicate lower
 361 likelihoods. The range across the SHAP value space indicates the degradation probability, expressed as
 362 the logarithm of the odds.

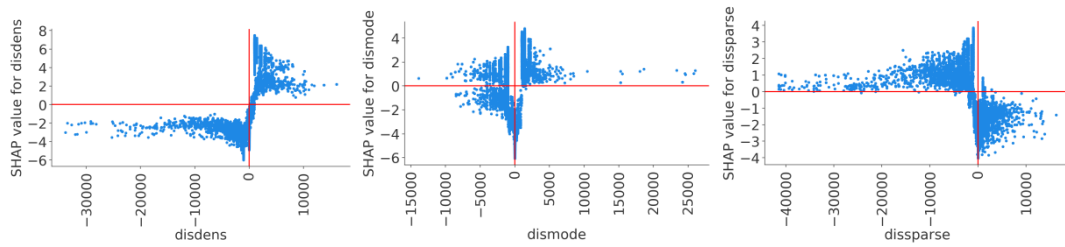
363 A recursive attribute elimination method was performed to determine how attribute reduction affects
 364 modelling performance using XGBoost with the oversampling method (see Fig. S 5; for more details,
 365 refer to Samardžić *et al.*, 2015). The results indicate that the first three drivers may already produce
 366 a satisfactory model ($\kappa = 0.74$, AUC-PR = 0.85, recall = 0.92), while adding the fourth driver can
 367 produce a robust model ($\kappa = 0.94$, AUC-PR = 0.98, recall = 0.98). This means that XGBoost used
 368 with the oversampling strategy can predict NGD with very high accuracy using a relatively small
 369 amount of data. Fig. S 6 shows the simulation result using the first four drivers, and compares the
 370 results with the observed map.

371 **3.3 Relationship between NGD and drivers in the XGBoost model**

372 SHAP values and spread (Figure 7) indicate that no linear relationship between driver and prediction
 373 could be found for any of the individual features. Change of distance to dense, moderately dense
 374 and sparse grass pixels, and change of sheep density were the dominant drivers for NGD. Figure 7a
 375 indicates that when $disdense < 0$, the SHAP value is negative, and when the distance to dense grass
 376 areas is small, the likelihood of degradation is also small. The relationship seems to be more
 377 complex for distance to moderately dense grass ($dismode$, Figure 7b); here, no simple linear
 378 interpretation is obvious. For distance to sparse grass ($dissparse$, Figure 7c), the pattern again
 379 suggests a rather linear interpretation, which is that the likelihood of degradation increases with
 380 decreasing distance. For sheep density, Figure 7d indicates that when sheep density decreased, the
 381 probability of GD obviously increased. Policy was not identified as a major driver of GD (Figure
 382 6). However, policy effects obviously have a different impact inside and outside sandy zones. Figure
 383 7e shows that our initial assumption is invalid: the probability of GD increased inside the sandy
 384 areas where we assumed effective policy measures to be in place (value 0). This result is also in line
 385 with Figure 7g, which shows that the closer to unused land, the more likely degradation will occur.

386 We can identify three groups for the remaining 14 drivers. For GDP and population density (Figure
 387 7g and Figure 7h), the likelihood of NGD increases with increasing values. Figure 7i-j indicate that
 388 warmer and drier climate conditions increase the probability of GD. Figure 7k, l, m and n indicate
 389 that the probability of GD rises with closer distances to forest, urban, rural and water areas. Figure
 390 7o shows a slight SHAP value pattern, in which the closer to cropland, the more unlikely degradation
 391 will occur. This is mainly due to transformation from cropland to grassland. Figure 7p-t do not show
 392 any interpretable spatial pattern.

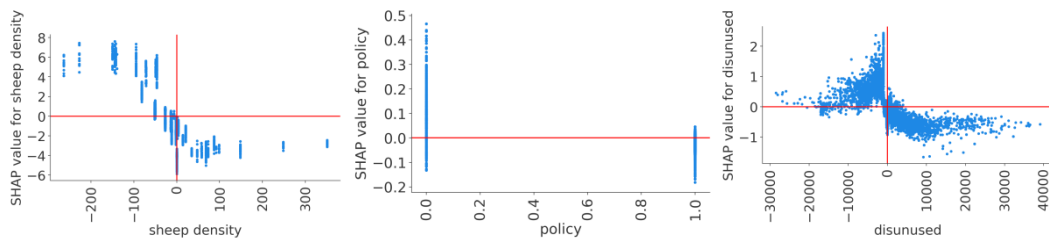
393



394

(a) (b) (c)

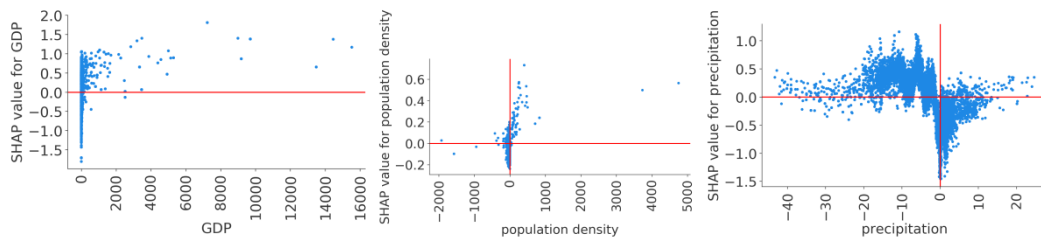
395



396

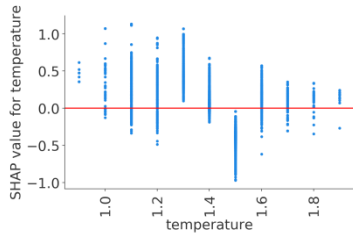
(d) (e) (f)

397

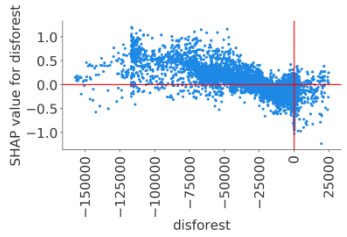


398

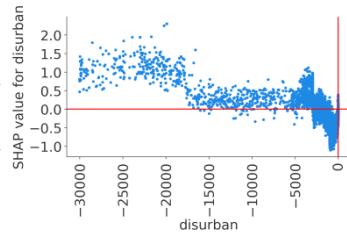
(g)



(h)



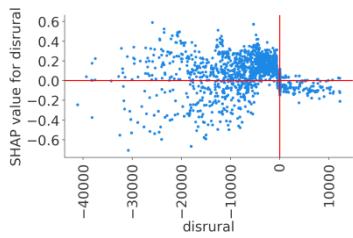
(i)



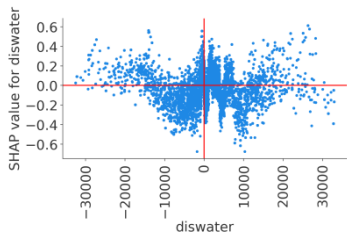
399

400

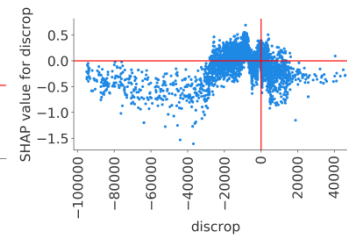
(j)



(k)



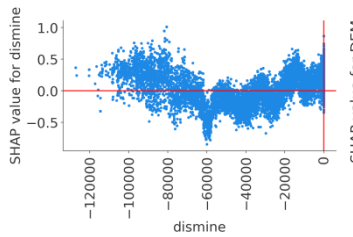
(l)



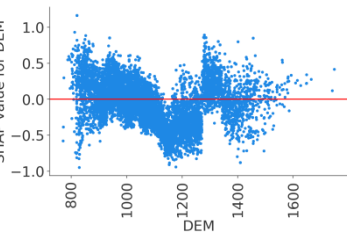
401

402

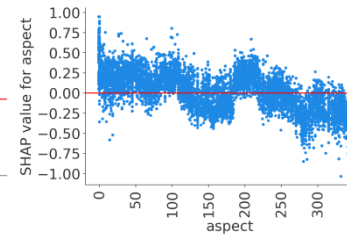
(m)



(n)



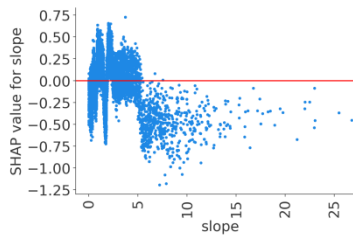
(o)



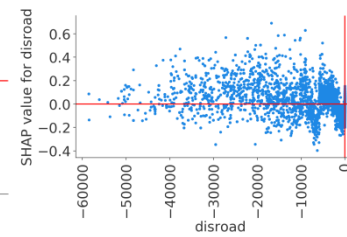
403

404

(p)



(q)

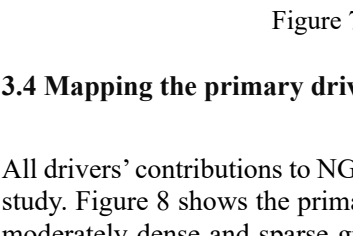


(r)

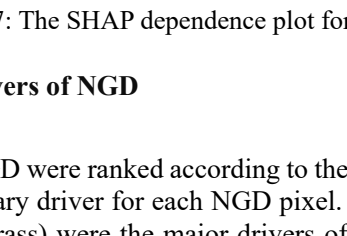
405

406

(s)



(t)



407

Figure 7: The SHAP dependence plot for each driver.

408

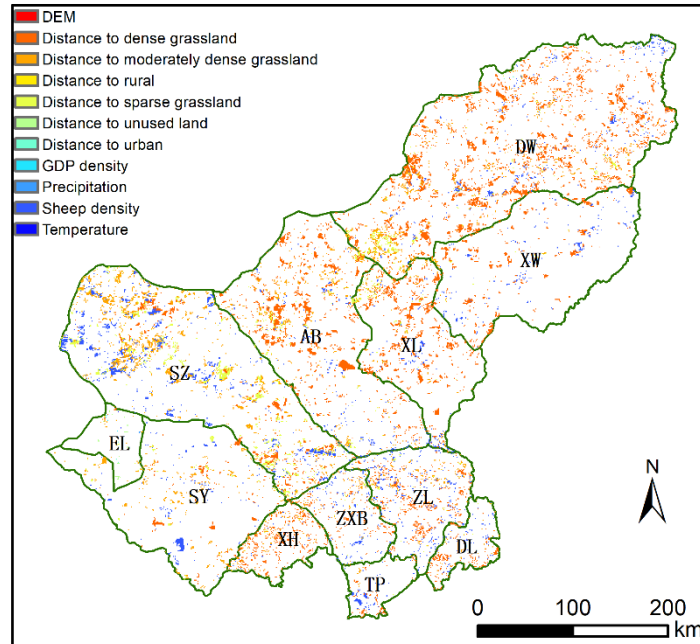
3.4 Mapping the primary drivers of NGD

409

All drivers' contributions to NGD were ranked according to their SHAP values for each pixel in this study. Figure 8 shows the primary driver for each NGD pixel. Distance to grassland pixels (dense, moderately dense and sparse grass) were the major drivers of NGD, responsible for 9,478, 3,892 and 1,629 NGD pixels, respectively. Sheep density was responsible for 3,042 NGD pixels, ranking third among all drivers. This order differs to that in Figure 6 and Figure 8 because in those cases, ranking is based on the total contribution of all drivers. Fig. S 7 shows the number of NGD pixels

414

415 in which a driver was dominant or primary. The change of distance to any type of grassland was the
 416 primary driver for about 82.8% of the total NGD pixels; sheep density accounted for 16.8%. The
 417 remaining seven drivers caused less than 1% of the total NGD. We can see from the spatial pattern
 418 that the change of distance to grassland was the major driver for GD in the dense grassland region
 419 (counties of DW, XL and AB), while in the counties of SZ, SY, ZXB, ZL and TP, sheep density was
 420 often identified as the major driver.



421

422

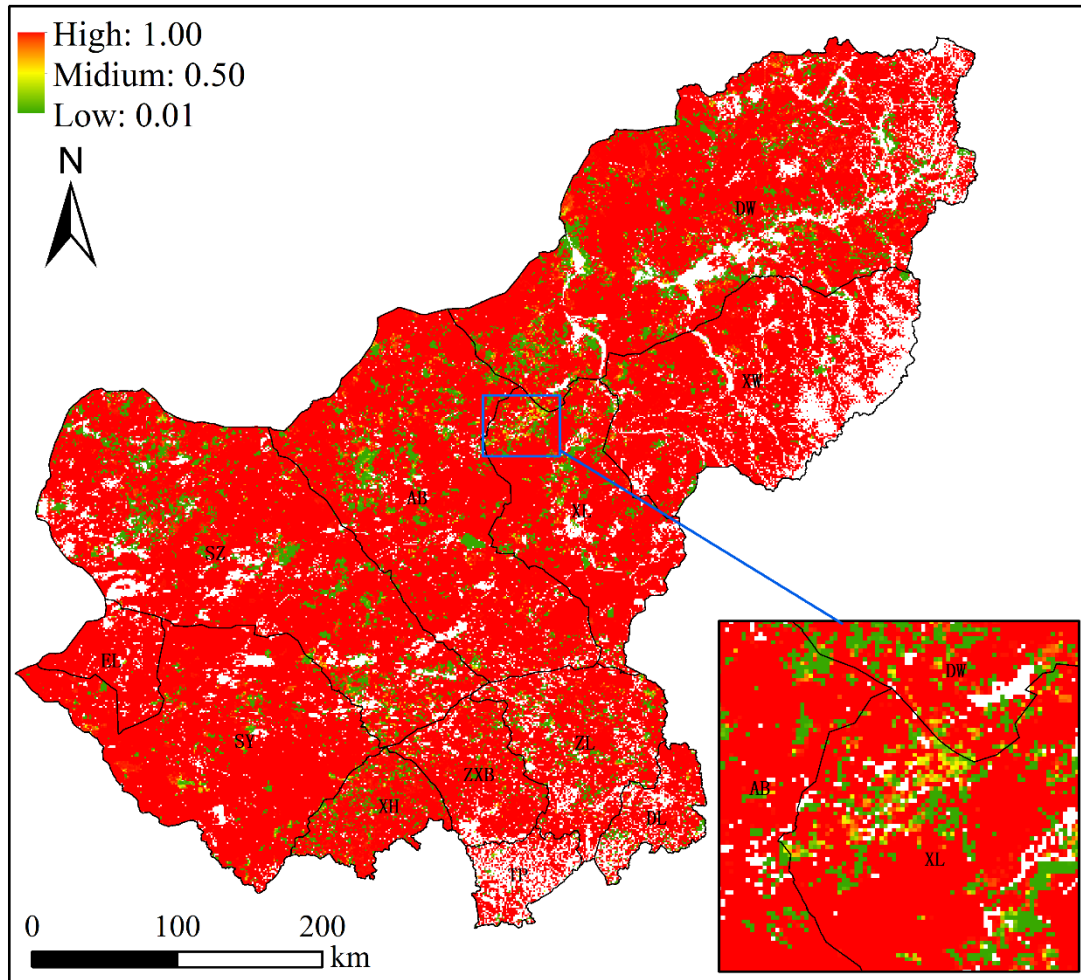
Figure 8: Spatial patterns of primary drivers for each pixel for NGD.

423

3.5 Regions of high risk for grassland degradation

424

A probability map of NGD was produced (Figure 9). Low probabilities of NGD were found in the
 425 central and northern counties (DW, XL, AB, SZ, ZL ZXB and XH), while high probability regions
 426 were EL, SY and XW. TP and DL in the south were categorised as low probability regions, due to
 427 their lower share of grassland area.



428

429 Figure 9: Degradation probability map for grassland in Xilingol, including a zoom into Xilinhot (XL)
 430 for more details. The probability is based on the four most important drivers.

431 4. Discussion

432 4.1 ML model building and evaluation

433 In this study, we defined a general framework for creating an ML model using the XGBoost
 434 algorithm for the purpose of analysing and predicting land-use change. XGBoost obtained a κ of
 435 93% and a recall value of > 99% when used to simulate and predict GD in this study. Compared to
 436 other popular ML learning algorithms, XGBoost exhibited a strong prediction ability. In studies
 437 where ANN, SVM, RF, CART, Multivariate Adaptive Regression Spline (MARS) or LR were used
 438 in combination with Cellular Automata (CA), the recall value is usually 54%-60% (Shafizadeh-
 439 Moghadam et al., 2017). Ahmadlou *et al.* (2019) stated that MARS and RF only yield high accuracy
 440 in training runs, but do not prove very accurate in the validating process when simulating land-use
 441 change.

442 Concerning the four sampling strategies we used to test the imbalance issue, we found that all
 443 strategies performed satisfactorily in the training runs. In the simulation, the under-sampling
 444 strategy yielded a relatively low accuracy ($\kappa = 0.46$) model. We assume that removal of data from

445 the majority class causes the model to lose the important concepts pertaining to the majority class
446 (He and Garcia, 2009). XGBoost used with the under-sampling method always produced similar
447 results, irrespective of the size of the dataset (see Fig. S 8). We conclude from this pattern that
448 XGBoost is also able to use sparse data to reflect real-world problems (Chen and Guestrin, 2016).

449 4.2 SHAP values and drivers of grassland degradation

450 The general idea of introducing SHAP values as a further tool to analyse XGBoost ranking is to
451 provide a method to evaluate the ranking with respect to causal relationships. The original XGBoost
452 ranking is based on the in-built feature selection functions *Gain* (refers to the improvement in
453 accuracy provided by a feature), *Weight* (or frequency, refers to the relative number of a feature
454 occurrence in the trees of a model) and *Coverage* (refers to the relative numbers of observations
455 related to this feature). However, these functions always produce different rankings of drivers (Abu-
456 Rmoleh, 2019) due to random components in the algorithms. SHAP values introduce two further
457 properties of feature importance measures: *consistency* (whenever we change a model such that it
458 relies more on a feature, the attributed importance for that feature should not decrease) and *accuracy*
459 (the sum of all feature importance values should equate to the total importance of the model;
460 Lundberg, 2018; Lundberg & Lee, 2017). Consistency is required to stabilise the ranking throughout
461 the analysis, reducing the change of order in the ranking to a minimum when the number of
462 identified drivers changes. The accuracy property of SHAP makes sure that each driver's
463 contribution to overall accuracy remains the same, even when drivers are excluded from analysis.
464 Other methods usually compensate for the withdrawal of a driver from the analysis, which makes
465 the determination of a single driver's contribution difficult.

466 The feature ranking based on SHAP values indicated that the change of distance to any type of
467 grassland (dense, moderately dense and sparse grass) is the most important driver for any newly
468 added grassland degradation. In this context, dense and moderately dense grassland areas are more
469 easily degraded than other land-use types, followed by sparse grass. These results are in line with
470 previous studies (Li et al., 2012; Xie and Sha, 2012). Good-quality grassland is more likely to be
471 degraded through increasing human disturbance. An explanation for this can be derived from local
472 people's living strategies. People who live in good-quality grassland areas are more likely to use
473 grassland for livestock production with higher animal densities, risking overgrazing. Furthermore,
474 Li et al. (2012) indicated that good-quality grassland is more likely to be converted to other land-
475 use types, such as cropland. In contrast, people who have lived in sparse grassland regions for
476 centuries have long adapted to low productivity, reducing their livestock numbers accordingly. They
477 have also developed strategies to cope with variability in weather conditions, e.g. by preparing and
478 storing more fodder and forage.

479 Sheep density was identified as the fourth major driver. However, the SHAP values indicate that
480 when sheep density decreases, the probability of grassland degradation increases. Overgrazing has
481 been the dominant driver for grassland degradation on the Mongolian plateau before, which has
482 changed the grassland ecosystem significantly towards lower grass coverage (Nkonya et al., 2016;
483 Wang et al., 2017). However, there is recent evidence that this causal relationship has changed. It
484 now appears that farmers increasingly select their livestock numbers according to the carrying
485 capacity of the grazing land (Cao et al., 2013b; Tiscornia et al., 2019b). By passing the "Fencing
486 Grassland and Moving Users" policy (FGMU), the Chinese government issued a law that regulates
487 livestock numbers based on a previously calculated carrying capacity. This development has
488 upturned the causal relationship between livestock numbers and NGD, reflected by the SHAP value
489 pattern in Figure 6.

490 Besides the four main drivers, seven other drivers also occasionally appear as the main driver for
491 some pixels (Figure 8). This highlights the fact that, at the local level, other drivers apart from the
492 four drivers identified as being major can also play a significant role. For example, in the county of

493 EL, the remaining seven drivers were mainly responsible for NGD. EL has less NGD after 2000
494 compared with other counties in Xilingol (Fig. S 1), and most of the EL area is covered by sparse
495 grass. EL is the most frequented border control point to Mongolia, and is subject to intensive tourism.

496 In the sparse grassland and agro-pastoral regions (SZ, SY, ZXB, ZL and TP), sheep density was
497 identified as the important driver. This indicates that, even though livestock numbers have decreased,
498 grassland is still experiencing serious degradation in this region. Here we see additional potential
499 for installing further grassland conservation measures, such as adjusting the livestock number to the
500 grassland carrying capacity.

501 **4.3 The current risk of grassland degradation in Xilingol**

502 Three regions of different risk classes were identified in the probability map of NGD (Fig. 9). The
503 low-risk region (DW, XL, AB, SZ, ZL ZXB and XH) is dominated by good-quality grassland (dense
504 and moderately dense grass). In recent decades, this region has suffered from increasing human
505 disturbance, e.g. overgrazing and mining development. However, after 2000, grassland in this region
506 has recovered, mainly as the result of ecological protection projects (Sun et al., 2017). Even though
507 this region is predicted as being less exposed to the risk of land degradation in the future, attention
508 is still required for the restoration process. The high-risk region includes the counties of EL, SY and
509 XW. EL and SY are covered by a large share of low-quality grassland, which – due to its own
510 fragility – is likely to be affected by extreme climate and human disturbance, more than, e.g. higher-
511 quality grasslands. The recent change in grassland property rights and the establishment of
512 ecological protection projects have also limited the mobility of nomadic herders throughout Xilingol.
513 As a consequence, herders cannot easily change grazing spots if extreme weather occurs; they are
514 then bound to have their cattle graze at the same spots, increasing the pressure on low-quality
515 grasslands in particular (Qian, 2011). For a long time, fragile grassland remained in an equilibrium
516 state with the extreme weather (frequent droughts, “dudz”) to which it was exposed, and with the
517 nomadic livestock husbandry that the region’s inhabitants practised. However, when the property
518 rights of grassland and livestock were changed from collective to private, the nomadic lifestyle was
519 largely abandoned.

520 **4.4 The limitations of XGBoost for scenario exploration**

521 XGBoost has already scored top in a range of algorithm competitions in the data scientists
522 community (Kaggle, 2019) due to its high accuracy and speed (Chen and Guestrin, 2016). ML
523 models extract patterns from data, without considering any existing expert knowledge, which is why
524 they are increasingly used to identify non-linear relationships (Ahmadlou et al., 2016; Samardžić-
525 Petrović et al., 2015; Tayyebi and Pijanowski, 2014b). However, ML models require specific data
526 structures for each problem to which they are applied. In this study, we simulated grassland
527 degradation in two different phases (1975-2000 and 2000-2015). All time series of driver data were
528 organised as model inputs, while grassland degradation dynamics were organised as prediction
529 targets. Although the model achieved high accuracy in predicting NGD in Phase 2, it was not
530 possible to achieve acceptable results in simulating both Phase 1 and Phase 2 separately. Second,
531 compared with conventional models, the XGBoost model cannot be easily transferred to other
532 regions for the same research question. Models like CLUE-S and GeoSOS-FLUS have been widely
533 used in different regions across the world (Fuchs et al., 2017; Liang et al., 2018a; Liu et al., 2017;
534 Verburg et al., 2002). When ML models are used in other regions, driver data must be collected and
535 structures adapted. Thirdly, ML models always need to learn sufficiently before they are able to
536 make predictions. This requires a sufficient amount of data covering historical periods or different
537 land-use change patterns.

538 XGBoost alone is unable to project any scenarios of land-use change based on historical data.
539 However, the methodology presented here can be applied to quantify alternative scenarios produced

540 using other approaches, such as conventional, rule-based models (Verburg et al., 2002) or cellular
541 automata (Islam et al., 2018; Shafizadeh-Moghadam et al., 2017).

542

543 **5 Conclusion**

544 Machine learning and data-driven approaches are becoming more and more important in many
545 research areas. The design and development of a practical land-use model requires both accuracy
546 and predictability to predict future land-use change, a well-fitted model that reflects and monitors
547 the real world (Ahmadlou et al., 2019). The method framework presented here for building an ML
548 model and explaining the relationship between drivers and grassland degradation identified
549 XGBoost as a robust data-driven model for this purpose. XGBoost showed higher accuracy in
550 training and simulation compared to existing ML models. Combined with over-sampling, it slightly
551 outperformed in the simulation process. The simulated map has a high agreement with the observed
552 values ($\kappa=93\%$).

553 We identified six basic steps that should be included in ML model building, and they are also similar
554 for other research applications (Kiyohara et al., 2018, 2018; Kontokosta and Tull, 2017;
555 Subramaniyan et al., 2018). However, different validation measures can be introduced in both the
556 training process and the simulation process. In this study, we tested different evaluation measures
557 to evaluate the ML model, e.g. a typical confusion matrix to evaluate the training process, AUC-PR
558 to evaluate the goodness of the ML model, and the kappa index to measure the degree of matching
559 between observed and simulated values. These validation indicators consider both the research
560 object and data characteristics. For example, when the data size is unbalanced, AUC-PR is a better
561 choice than AUC-ROC (Brownlee, 2018; Davis and Goadrich, 2006; Saito and Rehmsmeier, 2015).

562 SHAP was introduced in this context to provide a causal explanation of the patterns identified by
563 the ML model. In our case, SHAP was used to explain how drivers contribute to grassland
564 degradation processes at the pixel and regional level, despite their non-linear relationship.
565 According to the analysis, the distance to dense, moderately dense, and sparse grass, and sheep
566 density, were the most important drivers that caused new grassland degradation in this region. In
567 addition, individual SHAP values of sheep density indicated that the causal relationship between
568 grassland degradation and livestock pressure has changed over time: the increase in sheep density
569 was not the major driver for NGD in Phase 2 of the land degradation trajectory. Instead, the decrease
570 in the grazing capacity of grassland caused a decrease in livestock numbers. The primary driver map
571 of NGD provided a more detailed picture of NGD drivers for each pixel, as an important support
572 for grassland management in the Xilingol region. The individual SHAP values of each driver may
573 be an important prerequisite for rule-based scenario-building in the future.

574 **Author contribution:**

575 B prepared the manuscript with contribution from all co-authors. B gathered and prepared the data,
576 performed the simulations, and analysed the output. RW developed the model code. TL and CN
577 developed the research questions and the outline of the study.

578 **Code and data availability**

579 The development of XGBoost and SHAP values, graphs and model validation presented in this
580 paper were conducted using Python. The python script and related data have been published at
581 ZENODO (<https://zenodo.org/record/3937226#.Xw2M6egzZPY>).

582 The used XGBoost algorithm including the SHAP library runs well on a modern (Intel or AMD) PC
583 (4 cores or more, 16 GB RAM). The training and the simulation were made on Linux as operating
584 system but should work also under Windows.

585

586 **Competing interests:**

587 The authors declare that they have no conflict of interest

588 **Acknowledgements**

589 The authors express their sincere thanks to the China Scholarship Council (CSC) for funding this
590 research and to Elen Schofield for language editing.

591

592

593 **Reference**

594 Abdullah, A. Y. M., Masrur, A., Adnan, M. S. G., Baky, Md. A. A., Hassan, Q. K. and Dewan, A.:
595 Spatio-temporal Patterns of Land Use/Land Cover Change in the Heterogeneous Coastal Region of
596 Bangladesh between 1990 and 2017, *Remote Sens.*, 11(7), 790, doi:10.3390/rs11070790, 2019.

597 Abu-Rmieleh, A.: Be careful when interpreting your features importance in XGBoost!, *Data Sci.*
598 [online] Available from: <https://towardsdatascience.com/be-careful-when-interpreting-your-features-importance-in-xgboost-6e16132588e7> (Accessed 14 June 2019), 2019.

600 Ahmadlou, M., Delavar, M. R. and Tayyebi, A.: Comparing ANN and CART to Model Multiple
601 Land Use Changes: A Case Study of Sari and Ghaem-Shahr Cities in Iran, *JGST*, 6(1), 12, 2016.

602 Ahmadlou, M., Delavar, M. R., Basiri, A. and Karimi, M.: A Comparative Study of Machine
603 Learning Techniques to Simulate Land Use Changes, *J. Indian Soc. Remote Sens.*, 47(1), 53–62,
604 doi:10.1007/s12524-018-0866-z, 2019.

605 Akiyama, T. and Kawamura, K.: Grassland degradation in China: Methods of monitoring,
606 management and restoration, *Grassl. Sci.*, 53(1), 1–17, doi:10.1111/j.1744-697X.2007.00073.x,
607 2007.

608 Allington, G. R. H., Fernandez-Gimenez, M. E., Chen, J. and Brown, D. G.: Combining
609 participatory scenario planning and systems modeling to identify drivers of future sustainability on
610 the Mongolian Plateau, *Ecol. Soc.*, 23(2), art9, doi:10.5751/ES-10034-230209, 2018.

611 Anon: Resources and Environment Data Cloud Platform, Chinese Academic Science, [online]
612 Available from: <http://www.geodata.cn/> (Accessed 29 October 2018), 2018.

613 Batunacun and Ralf Wieland: XGBoost-SHAP values, prediction of grassland degradation, *Zenodo.*,
614 2020.

615 Batunacun, Wieland, R., Lakes, T., Yunfeng, H. and Nendel, C.: Identifying drivers of land
616 degradation in Xilingol, China, between 1975 and 2015, *Land Use Policy*, 83, 543–559,

- 617 doi:10.1016/j.landusepol.2019.02.013, 2019.
- 618 Bengtsson, J., Bullock, J. M., Egoh, B., Everson, C., Everson, T., O'Connor, T., O'Farrell, P. J.,
619 Smith, H. G. and Lindborg, R.: Grasslands-more important for ecosystem services than you might
620 think, *Ecosphere*, 10(2), e02582, doi:10.1002/ecs2.2582, 2019.
- 621 Brownlee, J.: How and When to Use ROC Curves and Precision-Recall Curves for Classification in
622 Python, *Mach. Learn. Mastery* [online] Available from: [https://machinelearningmastery.com/roc-
623 curves-and-precision-recall-curves-for-classification-in-python/](https://machinelearningmastery.com/roc-curves-and-precision-recall-curves-for-classification-in-python/) (Accessed 19 July 2019), 2018.
- 624 Cao, J., Yeh, E. T., Holden, N. M., Qin, Y. and Ren, Z.: The Roles of Overgrazing, Climate Change
625 and Policy As Drivers of Degradation of China's Grasslands, *Nomadic Peoples*, 17(2), 82–101,
626 doi:10.3167/np.2013.170207, 2013a.
- 627 Cao, J., Yeh, E. T., Holden, N. M., Qin, Y. and Ren, Z.: The Roles of Overgrazing, Climate Change
628 and Policy As Drivers of Degradation of China's Grasslands, *Nomadic Peoples*, 17(2), 82–101,
629 doi:10.3167/np.2013.170207, 2013b.
- 630 Cao, M., Zhu, Y., Quan, J., Zhou, S., Lü, G., Chen, M. and Huang, M.: Spatial Sequential Modeling
631 and Predication of Global Land Use and Land Cover Changes by Integrating a Global Change
632 Assessment Model and Cellular Automata, *Earths Future*, 7(9), 1102–1116,
633 doi:10.1029/2019EF001228, 2019.
- 634 Charif, O., Omrani, H., Abdallah, F. and Pijanowski, B.: A multi-label cellular automata model for
635 land change simulation, *Trans. GIS*, 21(6), 1298–1320, doi:10.1111/tgis.12279, 2017.
- 636 Chen, T. and Guestrin, C.: XGBoost: A Scalable Tree Boosting System, in *Proceedings of the 22nd
637 ACM SIGKDD International Conference on Knowledge Discovery and Data Mining - KDD '16*,
638 pp. 785–794, ACM Press, San Francisco, California, USA., 2016.
- 639 Dataman: Explain Your Model with the SHAP Values - Towards Data Science, *Data Sci.* [online]
640 Available from: [https://towardsdatascience.com/explain-your-model-with-the-shap-values-
641 bc36aac4de3d](https://towardsdatascience.com/explain-your-model-with-the-shap-values-bc36aac4de3d) (Accessed 8 October 2019), 2019.
- 642 Davis, J. and Goadrich, M.: The relationship between Precision-Recall and ROC curves, in
643 *Proceedings of the 23rd international conference on Machine learning - ICML '06*, pp. 233–240,
644 ACM Press, Pittsburgh, Pennsylvania., 2006.
- 645 Feng, Y., Liu, Y., Tong, X., Liu, M. and Deng, S.: Modeling dynamic urban growth using cellular
646 automata and particle swarm optimization rules, *Landscape Urban Plan.*, 102(3), 188–196,
647 doi:10.1016/j.landurbplan.2011.04.004, 2011.
- 648 Filippi, A. M., Güneralp, İ. and Randall, J.: Hyperspectral remote sensing of aboveground biomass
649 on a river meander bend using multivariate adaptive regression splines and stochastic gradient
650 boosting, *Remote Sens. Lett.*, 5(5), 432–441, doi:10.1080/2150704X.2014.915070, 2014.
- 651 Freeman, E. A., Moisen, G. G., Coulston, J. W. and Wilson, B. T.: Random forests and stochastic
652 gradient boosting for predicting tree canopy cover: comparing tuning processes and model
653 performance, *Can. J. For. Res.*, 46(3), 323–339, doi:10.1139/cjfr-2014-0562, 2016.
- 654 Fu, Q., Hou, Y., Wang, B., Bi, X., Li, B. and Zhang, X.: Scenario analysis of ecosystem service
655 changes and interactions in a mountain-oasis-desert system: a case study in Altay Prefecture, China,
656 *Sci. Rep.*, 8(1), doi:10.1038/s41598-018-31043-y, 2018.

- 657 Fuchs, R., Prestele, R. and Verburg, P. H.: A global assessment of gross and net land change
658 dynamics for current conditions and future scenarios, *Earth Syst. Dyn. Discuss.*, 1–29,
659 doi:10.5194/esd-2017-121, 2017.
- 660 Georganos, S., Grippa, T., Vanhuyse, S., Lennert, M., Shimoni, M. and Wolff, E.: Very High
661 Resolution Object-Based Land Use–Land Cover Urban Classification Using Extreme Gradient
662 Boosting, *IEEE Geosci. Remote Sens. Lett.*, 15(4), 607–611, doi:10.1109/LGRS.2018.2803259,
663 2018.
- 664 Gollnow, F. and Lakes, T.: Policy change, land use, and agriculture: The case of soy production and
665 cattle ranching in Brazil, 2001–2012, *Appl. Geogr.*, 55, 203–211, doi:10.1016/j.apgeog.2014.09.003,
666 2014.
- 667 Hao Dong, Xin Xu, Lei Wang and Fangling Pu: Gaofen-3 PolSAR Image Classification via
668 XGBoost and Polarimetric Spatial Information, *Sensors*, 18(2), 611, doi:10.3390/s18020611, 2018.
- 669 He, Shi, P., Li, X., Chen, J., Li, Y. and Li, J.: Developing Land Use Scenario Dynamics Model by
670 the Integration of System Dynamics Model and Cellular Automata Model, , 4, 2004.
- 671 He, H. and Garcia, E. A.: Learning from Imbalanced Data, *IEEE Trans. Knowl. Data Eng.*, 21(9),
672 1263–1284, doi:10.1109/TKDE.2008.239, 2009.
- 673 Hoffmann, C., Funk, R., Wieland, R., Li, Y. and Sommer, M.: Effects of grazing and topography on
674 dust flux and deposition in the Xilingele grassland, Inner Mongolia, *J. Arid Environ.*, 72(5), 792–
675 807, doi:10.1016/j.jaridenv.2007.09.004, 2008.
- 676 Huang, B., Xie, C., Tay, R. and Wu, B.: Land-Use-Change Modeling Using Unbalanced Support-
677 Vector Machines, *Environ. Plan. B Plan. Des.*, 36(3), 398–416, doi:10.1068/b33047, 2009.
- 678 Huang, B., Xie, C. and Tay, R.: Support vector machines for urban growth modeling,
679 *GeoInformatica*, 14(1), 83–99, doi:10.1007/s10707-009-0077-4, 2010.
- 680 Islam, K., Rahman, Md. F. and Jashimuddin, M.: Modeling land use change using Cellular Automata
681 and Artificial Neural Network: The case of Chunati Wildlife Sanctuary, Bangladesh, *Ecol. Indic.*,
682 88, 439–453, doi:10.1016/j.ecolind.2018.01.047, 2018.
- 683 Jacquin, A., Goulard, M., Hutchinson, J. M. S., Devienne, T. and Hutchinson, S. L.: A statistical
684 approach for predicting grassland degradation in disturbance-driven landscapes, *J. Environ. Prot.*,
685 7, 912–925, doi:10.4236/jep.2016.76081ff. fhal-01509642ff, 2016.
- 686 Kaggle: Kaggle: Your Home for Data Science, [online] Available from: <https://www.kaggle.com/>
687 (Accessed 5 January 2020), 2019.
- 688 Keshtkar, H., Voigt, W. and Alizadeh, E.: Land-cover classification and analysis of change using
689 machine-learning classifiers and multi-temporal remote sensing imagery, *Arab. J. Geosci.*, 10(6),
690 154, doi:10.1007/s12517-017-2899-y, 2017.
- 691 Khoury, A. E.: Modeling Land-Use Changes in the South Nation Watershed using Dyna-CLUE,
692 University of Ottawa, Ottawa, Canada. [online] Available from: <http://hdl.handle.net/10393/22902>,
693 2012.
- 694 Kiyohara, S., Miyata, T., Tsuda, K. and Mizoguchi, T.: Data-driven approach for the prediction and
695 interpretation of core-electron loss spectroscopy, *Sci. Rep.*, 8(1), 1–12, doi:10.1038/s41598-018-
696 30994-6, 2018.

- 697 Kontokosta, C. E. and Tull, C.: A data-driven predictive model of city-scale energy use in buildings,
698 *Appl. Energy*, 197, 303–317, doi:10.1016/j.apenergy.2017.04.005, 2017.
- 699 Krawczyk, B.: Learning from imbalanced data: open challenges and future directions, *Prog. Artif.*
700 *Intell.*, 5(4), 221–232, doi:10.1007/s13748-016-0094-0, 2016.
- 701 Krüger, C. and Lakes, T.: Bayesian belief networks as a versatile method for assessing uncertainty
702 in land-change modeling, *Int. J. Geogr. Inf. Sci.*, 29(1), 111–131,
703 doi:10.1080/13658816.2014.949265, 2015.
- 704 Kwon, H.-Y., Nkonya, E., Johnson, T., Graw, V., Kato, E. and Kihiu, E.: Global Estimates of the
705 Impacts of Grassland Degradation on Livestock Productivity from 2001 to 2011, in *Economics of*
706 *Land Degradation and Improvement – A Global Assessment for Sustainable Development*, edited
707 by E. Nkonya, A. Mirzabaev, and J. von Braun, pp. 197–214, Springer International Publishing,
708 Cham., 2016.
- 709 Lakes, T., Müller, D. and Krüger, C.: Cropland change in southern Romania: a comparison of
710 logistic regressions and artificial neural networks, *Landsc. Ecol.*, 24(9), 1195–1206,
711 doi:10.1007/s10980-009-9404-2, 2009.
- 712 Landis, J. R. and Koch, G. G.: The Measurement of Observer Agreement for Categorical Data,
713 *Biometrics*, 33(1), 159, doi:10.2307/2529310, 1977.
- 714 Li, S., Verburg, P. H., Lv, S., Wu, J. and Li, X.: Spatial analysis of the driving factors of grassland
715 degradation under conditions of climate change and intensive use in Inner Mongolia, China, *Reg.*
716 *Environ. Change*, 12(3), 461–474, doi:10.1007/s10113-011-0264-3, 2012.
- 717 Li, X. and Yeh, A. G.-O.: Neural-network-based cellular automata for simulating multiple land use
718 changes using GIS, *Int. J. Geogr. Inf. Sci.*, 16(4), 323–343, doi:10.1080/13658810210137004, 2002.
- 719 Li, X., Zhou, W. and Ouyang, Z.: Forty years of urban expansion in Beijing: What is the relative
720 importance of physical, socioeconomic, and neighborhood factors?, *Appl. Geogr.*, 38, 1–10,
721 doi:10.1016/j.apgeog.2012.11.004, 2013.
- 722 Li, X., Bai, Y., Wen, W., Wang, H., Li, R., Li, G. and Wang, H.: Effects of grassland degradation
723 and precipitation on carbon storage distributions in a semi-arid temperate grassland of Inner
724 Mongolia, China, *Acta Oecologica*, 85, 44–52, doi:10.1016/j.actao.2017.09.008, 2017.
- 725 Liang, X., Liu, X., Li, X., Chen, Y., Tian, H. and Yao, Y.: Delineating multi-scenario urban growth
726 boundaries with a CA-based FLUS model and morphological method, *Landsc. Urban Plan.*, 177,
727 47–63, doi:10.1016/j.landurbplan.2018.04.016, 2018a.
- 728 Liang, X., Liu, X., Li, D., Zhao, H. and Chen, G.: Urban growth simulation by incorporating
729 planning policies into a CA-based future land-use simulation model, *Int. J. Geogr. Inf. Sci.*, 32(11),
730 2294–2316, doi:10.1080/13658816.2018.1502441, 2018b.
- 731 Lin, Y., Deng, X., Li, X. and Ma, E.: Comparison of multinomial logistic regression and logistic
732 regression: which is more efficient in allocating land use?, *Front. Earth Sci.*, 8(4), 512–523,
733 doi:10.1007/s11707-014-0426-y, 2014.
- 734 Lin, Y.-P., Chu, H.-J., Wu, C.-F. and Verburg, P. H.: Predictive ability of logistic regression, auto-
735 logistic regression and neural network models in empirical land-use change modeling – a case study,
736 *Int. J. Geogr. Inf. Sci.*, 25(1), 65–87, doi:10.1080/13658811003752332, 2011.

- 737 Liu, M., Dries, L., Heijman, W., Zhu, X., Deng, X. and Huang, J.: Land tenure reform and grassland
738 degradation in Inner Mongolia, China, *China Econ. Rev.*, 55, 181–198,
739 doi:10.1016/j.chieco.2019.04.006, 2019.
- 740 Liu, X., Liang, X., Li, X., Xu, X., Ou, J., Chen, Y., Li, S., Wang, S. and Pei, F.: A future land use
741 simulation model (FLUS) for simulating multiple land use scenarios by coupling human and natural
742 effects, *Landsc. Urban Plan.*, 168, 94–116, doi:10.1016/j.landurbplan.2017.09.019, 2017.
- 743 Lundberg, S. M. and Lee, S.-I.: *A Unified Approach to Interpreting Model Predictions*, pp. 4768–
744 4777, Long Beach, California, USA., 2017.
- 745 Mileva Samardzic-Petrovic, Branislav Bajat, Miloš Kovačević and Suzana Dragicevic: Modelling
746 and analysing land use changes with data-driven models: a review of application on the Belgrade
747 study area, in *ResearchGate*, Belgrade. [online] Available from:
748 https://www.researchgate.net/publication/330910156_Modelling_and_analysing_land_use_changes_with_data-driven_models_a_review_of_application_on_the_Belgrade_study_area (Accessed 10
749 March 2019), 2018.
- 751 Mondal, I., Srivastava, V. K., Roy, P. S. and Talukdar, G.: Using logit model to identify the drivers
752 of landuse landcover change in the lower gangetic basin, india, *ISPRS - Int. Arch. Photogramm.*
753 *Remote Sens. Spat. Inf. Sci.*, XL–8, 853–859, doi:10.5194/isprsarchives-XL-8-853-2014, 2014.
- 754 Mustafa, A., Cools, M., Saadi, I. and Teller, J.: Coupling agent-based, cellular automata and logistic
755 regression into a hybrid urban expansion model (HUEM), *Land Use Policy*, 69, 529–540,
756 doi:10.1016/j.landusepol.2017.10.009, 2017.
- 757 Mustafa, A., Rienow, A., Saadi, I., Cools, M. and Teller, J.: Comparing support vector machines
758 with logistic regression for calibrating cellular automata land use change models, *Eur. J. Remote*
759 *Sens.*, 51(1), 391–401, doi:10.1080/22797254.2018.1442179, 2018.
- 760 National Research Council, N. R. C.: *Advancing Land Change Modeling: Opportunities and*
761 *Research Requirements*, National Academies Press, Washington, D.C., 2014.
- 762 Nkonya, E., Mirzabaev, A. and von Braun, J., Eds.: *Economics of Land Degradation and*
763 *Improvement – A Global Assessment for Sustainable Development*, Springer International
764 Publishing, Cham., 2016.
- 765 Pedregosa, F., Varoquaux, G., Gramfort, A., Michel, V., Thirion, B., Grisel, O., Blondel, M.,
766 Prettenhofer, P., Weiss, R., Dubourg, V., Vanderplas, J., Passos, A. and Cournapeau, D.: *Scikit-learn:*
767 *Machine Learning in Python*, *Mach. Learn. PYTHON*, 12, 2825–2830, 2011.
- 768 Pijanowski, B. C., Brown, D. G., Shellito, B. A. and Manik, G. A.: Using neural networks and GIS
769 to forecast land use changes: a Land Transformation Model, *Comput. Environ. Urban Syst.*, 26(6),
770 553–575, doi:10.1016/S0198-9715(01)00015-1, 2002.
- 771 Pijanowski, B. C., Pithadia, S., Shellito, B. A. and Alexandridis, K.: Calibrating a neural network-
772 based urban change model for two metropolitan areas of the Upper Midwest of the United States,
773 *Int. J. Geogr. Inf. Sci.*, 19(2), 197–215, doi:10.1080/13658810410001713416, 2005.
- 774 Qian, Z.: Herders' Social Vulnerability to Climate Change: A case of desert grassland in Inner
775 Mongolia (in Chinese), *Sociol. Study*, (6), 171–195, 2011.
- 776 Reiche, M.: *Wind erosion and dust deposition – A landscape in Inner Mongolia Grassland, China,*
777 *Universität Potsdam, Germany.*, 2014.

- 778 Ren, Y., Lü, Y., Comber, A., Fu, B., Harris, P. and Wu, L.: Spatially explicit simulation of land
779 use/land cover changes: Current coverage and future prospects, *Earth-Sci. Rev.*, 190, 398–415,
780 doi:10.1016/j.earscirev.2019.01.001, 2019.
- 781 Saito, T. and Rehmsmeier, M.: The Precision-Recall Plot Is More Informative than the ROC Plot
782 When Evaluating Binary Classifiers on Imbalanced Datasets, edited by G. Brock, *PLOS ONE*, 10(3),
783 e0118432, doi:10.1371/journal.pone.0118432, 2015.
- 784 Samardžić-Petrović, M., Dragičević, S., Bajat, B. and Kovačević, M.: Exploring the Decision Tree
785 Method for Modelling Urban Land Use Change, *GEOMATICA*, 69(3), 313–325,
786 doi:10.5623/cig2015-305, 2015.
- 787 Samardžić-Petrović, M., Dragičević, S., Kovačević, M. and Bajat, B.: Modeling Urban Land Use
788 Changes Using Support Vector Machines: Modeling Urban Land Use Changes Using Support
789 Vector Machines, *Trans. GIS*, 20(5), 718–734, doi:10.1111/tgis.12174, 2016.
- 790 Samardžić-Petrović, M., Kovačević, M., Bajat, B. and Dragičević, S.: Machine Learning Techniques
791 for Modelling Short Term Land-Use Change, *ISPRS Int. J. Geo-Inf.*, 6(12), 387,
792 doi:10.3390/ijgi6120387, 2017.
- 793 Samie, A., Deng, X., Jia, S. and Chen, D.: Scenario-Based Simulation on Dynamics of Land-Use-
794 Land-Cover Change in Punjab Province, Pakistan, *Sustainability*, 9(8), 1285,
795 doi:10.3390/su9081285, 2017.
- 796 Shafizadeh-Moghadam, H., Asghari, A., Tayyebi, A. and Taleai, M.: Coupling machine learning,
797 tree-based and statistical models with cellular automata to simulate urban growth, *Comput. Environ.*
798 *Urban Syst.*, 64, 297–308, doi:10.1016/j.compenvurbsys.2017.04.002, 2017.
- 799 Shao, L., Chen, H., Zhang, C. and Huo, X.: Effects of Major Grassland Conservation Programs
800 Implemented in Inner Mongolia since 2000 on Vegetation Restoration and Natural and
801 Anthropogenic Disturbances to Their Success, *Sustainability*, 9(3), 466, doi:10.3390/su9030466,
802 2017.
- 803 Sokolova, M. and Lapalme, G.: A systematic analysis of performance measures for classification
804 tasks, *Inf. Process. Manag.*, 45(4), 427–437, doi:10.1016/j.ipm.2009.03.002, 2009.
- 805 Su, H., Liu, W., Xu, H., Wang, Z., Zhang, H., Hu, H. and Li, Y.: Long-term livestock exclusion
806 facilitates native woody plant encroachment in a sandy semiarid rangeland, *Ecol. Evol.*, 5(12),
807 2445–2456, doi:10.1002/ece3.1531, 2015.
- 808 Subramaniyan, M., Skoogh, A., Salomonsson, H., Bangalore, P. and Bokrantz, J.: A data-driven
809 algorithm to predict throughput bottlenecks in a production system based on active periods of the
810 machines, *Comput. Ind. Eng.*, 125, 533–544, doi:10.1016/j.cie.2018.04.024, 2018.
- 811 Sun, B., Li, Z., Gao, Z., Guo, Z., Wang, B., Hu, X. and Bai, L.: Grassland degradation and restoration
812 monitoring and driving forces analysis based on long time-series remote sensing data in Xilin Gol
813 League, *Acta Ecol. Sin.*, 37(4), 219–228, doi:10.1016/j.chnaes.2017.02.009, 2017.
- 814 Sun, Z. and Müller, D.: A framework for modeling payments for ecosystem services with agent-
815 based models, Bayesian belief networks and opinion dynamics models, *Environ. Model. Softw.*, 45,
816 15–28, doi:10.1016/j.envsoft.2012.06.007, 2013.
- 817 Tayyebi, A. and Pijanowski, B. C.: Modeling multiple land use changes using ANN, CART and
818 MARS: Comparing tradeoffs in goodness of fit and explanatory power of data mining tools, *Int. J.*

- 819 Appl. Earth Obs. Geoinformation, Complete(28), 102–116, doi:10.1016/j.jag.2013.11.008, 2014a.
- 820 Tayyebi, A. and Pijanowski, B. C.: Modeling multiple land use changes using ANN, CART and
821 MARS: Comparing tradeoffs in goodness of fit and explanatory power of data mining tools, Int. J.
822 Appl. Earth Obs. Geoinformation, 28, 102–116, doi:10.1016/j.jag.2013.11.008, 2014b.
- 823 Tiscornia, G., Jaurena, M. and Baethgen, W.: Drivers, Process, and Consequences of Native
824 Grassland Degradation: Insights from a Literature Review and a Survey in Río de la Plata Grasslands,
825 Agronomy, 9(5), 239, doi:10.3390/agronomy9050239, 2019a.
- 826 Tiscornia, G., Jaurena, M. and Baethgen, W.: Drivers, Process, and Consequences of Native
827 Grassland Degradation: Insights from a Literature Review and a Survey in Río de la Plata Grasslands,
828 Agronomy, 9(5), 239, doi:10.3390/agronomy9050239, 2019b.
- 829 Tong, S., Bao, Y., Te, R., Ma, Q., Ha, S. and Lusi, A.: Analysis of Drought Characteristics in Xilingol
830 Grassland of Northern China Based on SPEI and Its Impact on Vegetation, Math. Probl. Eng., 2017,
831 1–11, doi:10.1155/2017/5209173, 2017.
- 832 Troost, C., Walter, T. and Berger, T.: Climate, energy and environmental policies in agriculture:
833 Simulating likely farmer responses in Southwest Germany, Land Use Policy, 46, 50–64,
834 doi:10.1016/j.landusepol.2015.01.028, 2015.
- 835 Verburg, P. H. and Chen, Y.: Multiscale Characterization of Land-Use Patterns in China, Ecosystems,
836 3(4), 369–385, doi:10.1007/s100210000033, 2000.
- 837 Verburg, P. H. and Veldkamp, A.: Projecting land use transitions at forest fringes in the Philippines
838 at two spatial scales, Landsc. Ecol., 19(1), 77–98, doi:10.1023/B:LAND.0000018370.57457.58,
839 2004.
- 840 Verburg, P. H., Soepboer, W., Veldkamp, A., Limpiada, R., Espaldon, V. and Mastura, S. S. A.:
841 Modeling the Spatial Dynamics of Regional Land Use: The CLUE-S Model, Environ. Manage.,
842 30(3), 391–405, doi:10.1007/s00267-002-2630-x, 2002.
- 843 Vermeiren, K., Vanmaercke, M., Beckers, J. and Van Rompaey, A.: ASSURE: a model for the
844 simulation of urban expansion and intra-urban social segregation, Int. J. Geogr. Inf. Sci., 30(12),
845 2377–2400, doi:10.1080/13658816.2016.1177641, 2016.
- 846 Vluymans, S.: Learning from Imbalanced Data, in Dealing with Imbalanced and Weakly Labelled
847 Data in Machine Learning using Fuzzy and Rough Set Methods, vol. 807, pp. 81–110, Springer
848 International Publishing, Cham., 2019.
- 849 Wang, X., Dong, S., Yang, B., Li, Y. and Su, X.: The effects of grassland degradation on plant
850 diversity, primary productivity, and soil fertility in the alpine region of Asia's headwaters, Environ.
851 Monit. Assess., 186(10), 6903–6917, doi:10.1007/s10661-014-3898-z, 2014.
- 852 Wang, Y., Wang, Z., Li, R., Meng, X., Ju, X., Zhao, Y. and Sha, Z.: Comparison of Modeling
853 Grassland Degradation with and without Considering Localized Spatial Associations in Vegetation
854 Changing Patterns, Sustainability, 10(2), 316, doi:10.3390/su10020316, 2018.
- 855 Wang, Z., Deng, X., Song, W., Li, Z. and Chen, J.: What is the main cause of grassland degradation?
856 A case study of grassland ecosystem service in the middle-south Inner Mongolia, CATENA, 150,
857 100–107, doi:10.1016/j.catena.2016.11.014, 2017.
- 858 Xie, Y. and Sha, Z.: Quantitative Analysis of Driving Factors of Grassland Degradation: A Case

- 859 Study in Xilin River Basin, Inner Mongolia, *Sci. World J.*, 2012, 1–14, doi:10.1100/2012/169724,
860 2012.
- 861 Xu GC, Kang MY, Marc Metzger and Y Jiang: Vulnerability of the Human-Environment System in
862 Arid Regions: The Case of Xilingol Grassland in Northern China, *Pol. J. Environ. Stud.*, 23(5),
863 1773–1785, 2014.
- 864 Yang, J., Chen, F., Xi, J., Xie, P. and Li, C.: A Multitarget Land Use Change Simulation Model
865 Based on Cellular Automata and Its Application, *Abstr. Appl. Anal.*, 2014, 1–11,
866 doi:10.1155/2014/375389, 2014.
- 867 Yang, X., Chen, R. and Zheng, X. Q.: Simulating land use change by integrating ANN-CA model
868 and landscape pattern indices, *Geomat. Nat. Hazards Risk*, 7(3), 918–932,
869 doi:10.1080/19475705.2014.1001797, 2016.
- 870 Zhan J Y, Xiangzheng Deng, Ou Jiang and Nana Shi: The Application of System Dynamics and
871 CLUE-S Model in Land Use Change Dynamic Simulation: a Case Study in Taips County, Inner
872 Mongolia of China, in *Management Science*, pp. 2781–2790, Shanghai. [online] Available from:
873 [https://www.researchgate.net/publication/228986766_The_Application_of_System_Dynamics_and](https://www.researchgate.net/publication/228986766_The_Application_of_System_Dynamics_and_CLUE-S_Model_in_Land_Use_Change_Dynamic_Simulation_a_Case_Study_in_Taips_County_Inner_Mongolia_of_China)
874 [CLUE-](https://www.researchgate.net/publication/228986766_The_Application_of_System_Dynamics_and_CLUE-S_Model_in_Land_Use_Change_Dynamic_Simulation_a_Case_Study_in_Taips_County_Inner_Mongolia_of_China)
875 [S_Model_in_Land_Use_Change_Dynamic_Simulation_a_Case_Study_in_Taips_County_Inner_](https://www.researchgate.net/publication/228986766_The_Application_of_System_Dynamics_and_CLUE-S_Model_in_Land_Use_Change_Dynamic_Simulation_a_Case_Study_in_Taips_County_Inner_Mongolia_of_China)
876 [Mongolia_of_China](https://www.researchgate.net/publication/228986766_The_Application_of_System_Dynamics_and_CLUE-S_Model_in_Land_Use_Change_Dynamic_Simulation_a_Case_Study_in_Taips_County_Inner_Mongolia_of_China) (Accessed 29 April 2018), 2007.
- 877 Zhang, M., Zhao, J. and Yuan, L.: Simulation of Land-Use Policies on Spatial Layout with the
878 CLUE-S Model, *ISPRS - Int. Arch. Photogramm. Remote Sens. Spat. Inf. Sci.*, XL-2/W1, 185–190,
879 doi:10.5194/isprsarchives-XL-2-W1-185-2013, 2013.
- 880
- 881